Molecular Therapy
Nucleic Acids
Original Article

Synergic microRNAs suppress human glioblastoma progression by modulating clinically relevant targets

Silvia Rancati,[1] Rui C. Pereira,[1,7] Michele Schlich,[2,7] Stefania Sgroi,[1] Silvia Beatini,[1] Letizia La Rosa,[1] Lidia Giantomasi,[1] Roberta Pelizzoli,[1] Clarissa Braccia,[3] Andrea Di Fonzo,[3] Carlotta Spattini,[1,4] Kiril Tuntevski,[1,4] Amanda Lo Van,[1] Meritxell Pons-Espinal,[1] Annalisa Palange,[2] Adriana Bajetto,[5] Antonio Daga,[6] Andrea Armirotti,[3] Tullio Florio,[5,6] Paolo Decuzzi,[2] and Davide De Pietri Tonelli[1]

[1]Neurobiology of miRNAs, Istituto Italiano di Tecnologia, 16163 Genoa, Italy; [2]Nanotechnology for Precision Medicine, Istituto Italiano di Tecnologia, 16163 Genoa, Italy; [3]Analytical Chemistry, Istituto Italiano di Tecnologia, 16163 Genoa, Italy; [4]Open University Affiliated Research Centre at Istituto Italiano di Tecnologia (ARC@IIT), 16163 Genoa, Italy; [5]Section of Pharmacology, Department of Internal Medicine, University of Genoa, 16132 Genoa, Italy; [6]IRCCS Policlinico San Martino, 16132 Genoa, Italy

Glioblastoma (GBM) is a highly aggressive brain tumor characterized by therapy-resistant glioma stem-like cells (GSCs) and extensive infiltration into surrounding brain tissue. MicroRNAs (miRNAs) are pleiotropic post-transcriptional regulators of oncogenic pathways, but their tumor-suppressive function is frequently lost in GBM. This study explores a multimodal therapeutic approach by restoring a combination of miRNAs to exploit their synergistic effects against GBM. Using patient-derived GBM cells cultured under stem cell-permissive conditions, we demonstrate that miRNA restoration reduces tumor growth, limits invasiveness and stemness, and enhances sensitivity to temozolomide (TMZ). *In vivo* studies in an orthotopic xenograft mouse model of GBM confirm the therapeutic efficacy and low toxicity of the nanoformulated miRNAs, following local injection. Multi-omics and computational analyses on different GBM subtypes reveal that these miRNAs synergistically suppress tumor-promoting extracellular matrix interactions, particularly through the collagen pathway, and downregulate genes associated with GBM progression. The genes downregulated by the miRNAs correlate with glioma grade and poor patient prognosis, further underscoring their therapeutic potential. These findings highlight the promise of combinatorial miRNA therapy as a novel strategy for GBM treatment and suggest new molecular targets for future diagnostic and therapeutic developments.

INTRODUCTION

Glioblastoma (GBM) is the most common and aggressive malignant brain tumor in adults, with a median survival of approximately 14.5 months, a figure that unfortunately has not improved over the past two decades.[1] Recurrence is the unavoidable outcome of GBM, likely driven by therapy-resistant, heterogeneous glioma stem-like cell (GSC) subpopulations, which are reminiscent of neural stem cells (NSCs).[2,3] This is in line with the hypothesis that GBM may originate from the malignant transformation of NSCs.[3–5] GSCs are predominantly quiescent and infiltrate the non-neoplastic brain parenchyma, complicating surgical resection and resulting in the development of therapy-resistant clones following standard-of-care treatments.[6,7] Moreover, as confirmed by the limited success of therapeutic strategies aimed at one or few targets, GBM is unlikely to be cured by targeting one or few factors, in line with the notion that cancer is not a unique disease caused by a single mutation or epigenetic alteration.[8] Thereby, the identification of effective multimodal therapies, ideally aimed at GSC depletion and preventing infiltration, is an urgent need for this malignancy.

MicroRNAs (miRNAs) are small noncoding RNAs that by post-transcriptional repression of the majority of protein-coding genes in mammals maintain proper transcriptional homeostasis.[9–11] Since the original report of miRNA dysregulation in cancer, several studies have shown that this is also the case in glioma, in line with the aberrant activation of genetic programs in this malignancy.[12–15] Unsurprisingly, miRNAs are regarded as promising tools and targets for cancer therapy.[16] However, despite various miRNA-based drugs have been included in clinical trials, many of those targeting single miRNAs have failed, indicating a need for further development.[17] Conversely, the use of miRNA combinations has recently gained momentum as a therapeutic strategy in neuro-oncology, in line with the functional redundancy (i.e., synergism) of miRNAs in physiological NSCs.[13,18–23]

Received 10 March 2025; accepted 31 October 2025;
https://doi.org/10.1016/j.omtn.2025.102763.

[7]These authors contributed equally

Correspondence: Davide De Pietri Tonelli, Istituto Italiano di Tecnologia (IIT), Via Morego 30, 16163 Genova, Italy.
E-mail: davide.depietri@iit.it

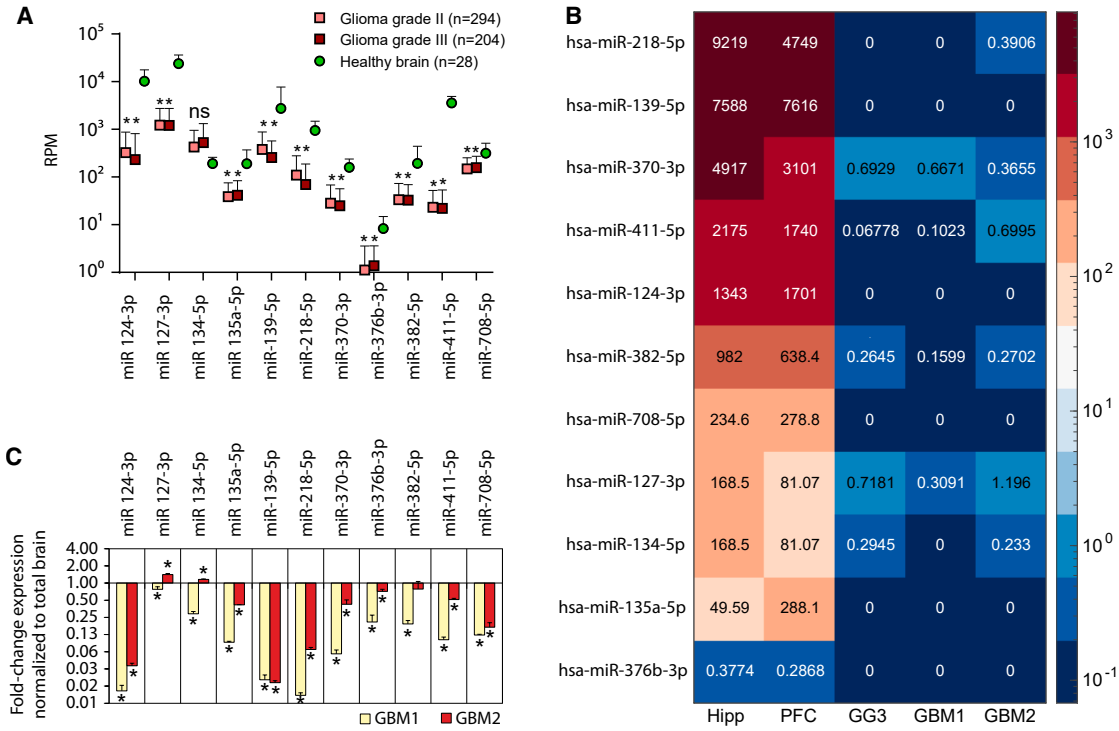

Figure 1. Underexpression of the 11 miRNAs in gliomas of different grades

(A) Levels of the 11 miRNAs in glioma samples (from TCGA-LGG cohort: $n = 294$ grade II and $n = 204$ grade III glioma) and non-neoplastic brain tissue ($n = 28$). Data expressed as reads per million (average ±SD; $^*p < 0.001$, unpaired t test). (B) Heatmap of small RNA-seq showing levels of the 11 miRNAs in the cell cultures from two GBM patients (GBM1, 2), in glioma grade III cells (GG3), and non-neoplastic human hippocampus (Hipp) and prefrontal cortex (PFC) from GEO database accession # PRJNA752352 and GSE181520). Data are the mean TPM in $n = 3$ biological triplicates. (C) Quantification (qPCR) of abundances of the 11 miRNAs in GBM1 and GBM2 cultures normalized to non-neoplastic brain RNA (data are the mean ΔΔct ±SD of $n = 1$ experiment in technical triplicate; two-tailed t test $^*p < 0.05$).

We previously identified a set of 11 pro-neurogenic miRNAs (henceforth "the POOL") that sustains adult neurogenesis through the synergistic modulation of different targets in mouse NSCs.[24] Since the rescued miRNA POOL was sufficient to restore impaired neurogenesis in miRNA-depleted NSCs, which resemble GSCs, and given that the 11 miRNA sequences are conserved between mouse and human, we hypothesized that this POOL might be effective against GBM. Here, we study the expression of the 11 miRNAs across various glioma grades and GBM subtypes in patients and demonstrate the efficacy of the POOL as a gene therapy against GBM. Finally, by multi-omics analysis, we infer the mechanisms underlying the tumor-suppressive functions of the POOL in different GBM subtypes and uncover that these miRNAs suppress clinically relevant targets in glioma.

RESULTS

Underexpression of the 11 miRNAs in gliomas of different grades

To correlate the abundance of the 11 miRNAs (i.e., miR-124-3p, miR-127-3p, miR-134-5p, miR-135a-5p, miR-139-5p, miR-218-5p, miR-370-3p, miR-376b-3p, miR-382-5p, miR-411-5p, and miR-708-5p sequences in Table S1) with human glioma grade, we analyzed public datasets of low-grade glioma (LGG) from The Cancer Genome Atlas (TCGA), available in the DIANA-miTED database, and of non-neoplastic human brain, as control.[25,26] Ten of the 11 miRNAs (except miR-134-5p) are significantly underexpressed in grade II and grade III gliomas compared to controls (Figure 1A). Because grade IV glioma (i.e., GBM) was not available in this dataset, abundance of the 11 miRNAs was quantified by small RNA sequencing (RNA-seq) and quantitative real-time PCR (real-time qPCR) in cultures obtained from surgical samples of patients with glioma grade III (GG3) and GBM (GBM1 and 2).[27] This analysis indicated that the 11 miRNAs are underexpressed in two grade IV gliomas (GBM1, classified as proneural, and GBM2, classified as the mesenchymal subtype, respectively; *S.R. unpublished data*) and in one GG3, compared to non-neoplastic controls (Figure 1B, statistics in Table S2).[27] Real-time qPCR confirmed that 11 and nine of the miRNAs were underexpressed in GBM1 and GBM2, respectively, compared with control brain (Figure 1C). These results, indicating variations in the abundances of the 11 miRNAs across distinct GBM grades and subtypes, are in line with the heterogeneity of this malignancy and suggest that underexpression of these miRNAs is likely associated with gliomagenesis and/or tumor progression.

The POOL significantly reduces GBM growth and invasiveness and increases sensitivity to TMZ

To determine whether the POOL elicits a phenotypic effect in GBM, we transfected synthetic mimics of the 11 miRNAs in equimolar concentrations (i.e., 25 nM each of the 11 miRNAs) or a scrambled RNA mimic (control) to a final concentration of 250 nM in both patient-derived GBM cultures and cultured them as monolayers. Rescued expression of the 11 miRNAs was confirmed by real-time qPCR 5 h after transfection (*black bars* in Figure 5A). We performed a scratch-wound assay combined with label-free automated live imaging to quantify migration (cells migrating on plastic), invasion (cells penetrating a Matrigel layer) (Figure 2A), and growth (cell confluence; Figure 2B) in both GBM cultures. Treatment with the POOL did not affect migration in either GBM culture (Figure 2A), but it significantly reduced invasion in GBM2, while having no effect in GBM1 (Figure 2A). Interestingly, cell growth was reduced in both GBM cultures following POOL treatment (Figure 2B). Hence, the POOL can significantly reduce GBM growth and invasiveness *in vitro*, suggesting it may be more effective in the mesenchymal (GBM2) rather than in the proneural (GBM1) subtype.

Given the observed heterogeneity in the miRNA abundances across different GBM subtypes (Figure 1), we asked whether all the miRNAs are required to elicit the aforementioned effects in GBM. To address this question, we quantified the growth of GBM2 cells upon the transfection of the POOL with all the 11 miRNAs (POOL) or 11 combinations, each missing one of the miRNAs (POOL minus "miR-*x*"), versus scrambled RNA (Figure 2C, control). Quantification of cell confluence at 72 h indicated an attenuation of the effect for eight sub-pool combinations on GBM2 growth (Figure 2C). This result suggested that a subset of miRs may be sufficient to rescue proliferation. However, different combinations may be needed to tune distinct phenotypes, such as those involved in adhesion or migration, which are also critical in GBM pathology. Thereby, we chose to retain the full POOL for the subsequent experiments, in line with our previous findings in NSCs.[24]

To validate the effects of the POOL in a GBM model, which better mimics the 3D features and interaction of the tumor with the microenvironment, we formed spheroids of GBM from cells that were pre-transfected with the POOL or scrambled RNA, and then we followed their growth and infiltration upon embedding them in collagen hydrogels.[28] In contrast to cells cultured in monolayers, the POOL did not alter growth of the spheroid core area (*dashed circles* in Figure 2D) compared to scrambled control, whereas the invasion area (i.e., the surface occupied by cells protruding out of the core, *white lines* in Figure 2D) was significantly reduced in both GBM cultures upon transfection with the POOL; again, a stronger inhibition of infiltration was observed upon POOL treatment in the mesenchymal GBM2, compared to proneural GBM1 subtype (Figure 2E).

To assess the efficacy of the POOL in combination with chemotherapy, POOL- or scrambled-transfected GBM1 and GBM2 were cultured in the presence of increasing TMZ concentrations (1:2 dilutions ranging from 1,500 to 46 μM), and growth was documented by imaging for up to 72 h (Figure S1). Remarkably, the POOL increased TMZ sensitivity of GBM1 (but not of GBM2, *not shown*) compared to scrambled RNA (Figure S1).

Together, these results demonstrate that the POOL has a tumor-suppressive role in GBM, primarily by reducing invasiveness, and suggest that these miRNAs may likely enhance GBM sensitivity to TMZ.

The POOL represses the collagen pathway and markers of GSC subpopulation

To gain a mechanistic insight, we sought to identify genes and pathways regulated by the POOL in GBM. Therefore, we performed liquid chromatography-mass spectrometry (LC-MS) proteomics and RNA-seq to shed light on the effects of the 11 miRNAs on the proteome and transcriptome, respectively. POOL- and scrambled-transfected spheroids of both GBM subtypes, a condition previously shown to preserve GSCs and tumor-initiating properties, were harvested after 3 or 6 days, for RNA-seq and proteomics, respectively.[27,29] Untargeted proteomics identified ∼4,000 unique proteins expressed in each of the two POOL-transfected or scrambled-transfected GBM cultures (3,962 in GBM1; 4,206 in GBM2). The POOL significantly altered 8.8% and 11% of proteins in GBM1 and GBM2 (false discovery rate [FDR] < 0.05), respectively, compared to scrambled-transfected controls (Table S3). Principal-component analysis of the proteomics data indicated a clear segregation of the two GBM cultures along the PC1 (Figure S2), in agreement with the heterogeneity that characterizes this malignancy and with the different gene expression profiles of the two samples.[6,30] Consistently, with the observed tumor-suppressive effect of the POOL, we found an evident segregation of POOL- and scrambled-transfected GBM samples along PC2 (Figure S2). Analogously, by RNA-seq we found that the POOL significantly altered 4% and 5.9% transcripts (FDR < 0.05) in GBM1 and GBM2, respectively (Table S4). These results indicate that the POOL modulates a substantial portion of the proteome and transcriptome in different GBMs.

Given that miRNAs act mostly as repressors, to identify the possible mechanisms underlying the tumor-suppressive functions of the POOL, we focused on genes and proteins downregulated in both GBM cultures (Figure 3A). As expected for such heterogeneous malignancy, most of the downregulated genes and proteins were different between the two cultures. Interestingly, 37 of them were commonly downregulated in both GBM cultures at the transcript or protein levels (Figure 3A, *top*). Among them, PLOD3, MMP14, NQO1, and several members of collagen IV and integrin family were suppressed by the POOL in both GBM cultures (Figure 3A, *top*). Indeed, despite the inherent differences between the two GBM subtypes, Gene Ontology (GO) analysis indicated that the POOL suppresses similar pathways in both GBM models, particularly cell adhesion and cell membrane mediators of the extracellular matrix (ECM) interaction and production, with several pathways being shared between proteomics and transcriptomics datasets

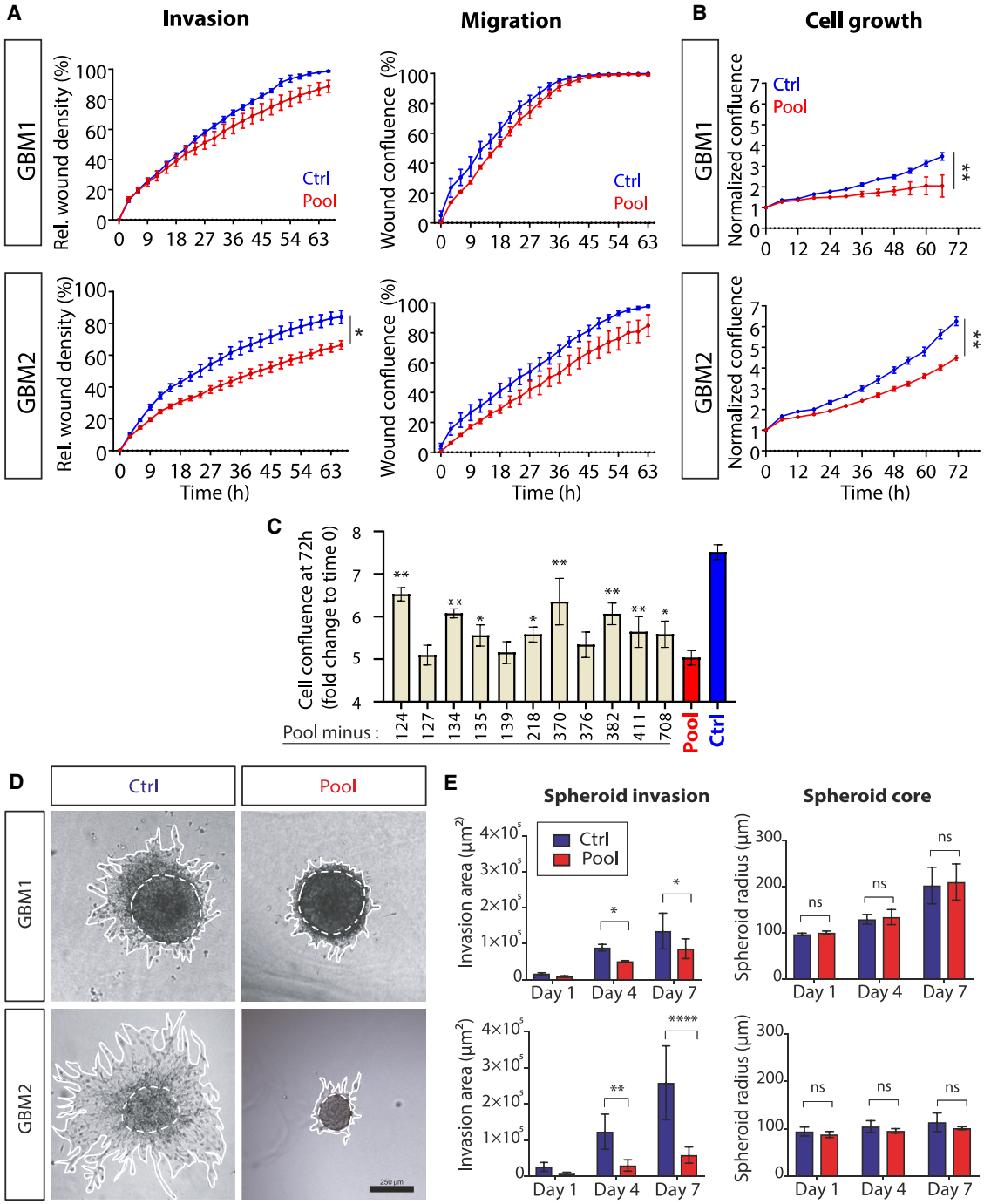

Figure 2. The POOL significantly reduces GBM growth and invasiveness

(A) Scratch-wound assay quantification of invasion or migration of scrambled RNA (ctrl) and POOL-transfected GBM 1, 2 (data are mean ± SEM of $n = 1$ experiment, in triplicate, two-way ANOVA interaction p value (time × treatment): $^{*}p < 0.05$). (B) Quantification of growth of scrambled RNA ("ctrl") and POOL-transfected GBM1, 2 (mean ± SEM of $n = 1$ experiment; five replicates; two-way ANOVA interaction p value (time × treatment) $^{**}p < 0.005$). (C) Growth of scrambled RNA (ctrl), POOL or subPOOL each missing one miRNA measured at 72 h upon transfection. The missing miRNA is indicated in the x axis ($n = 1$ experiment, five replicates; asterisks mark statistical significance of each condition versus POOL: $^{*}p < 0.05$, $^{**}p < 0.005$; one-way ANOVA and multiple comparisons; all the tested conditions are statistically significant when compared to scrambled). (D and E) Representative images and plots showing spheroids from scrambled RNA (ctrl) and POOL-transfected GBM1 and GBM2 after 7 days in 3D collagen; quantification of spheroid cores (*dashed circles*) and invasion area (*delimited by the dashed and the white line*). Scale bars, 250 µm (data are expressed as means ± SD of $n > 3$ independent experiments, each with $n > 5$ spheroids per condition; two-way ANOVA and multiple comparisons: $^{*}p < 0.05$; $^{**}p < 0.005$ $^{****}p < 0.0001$).

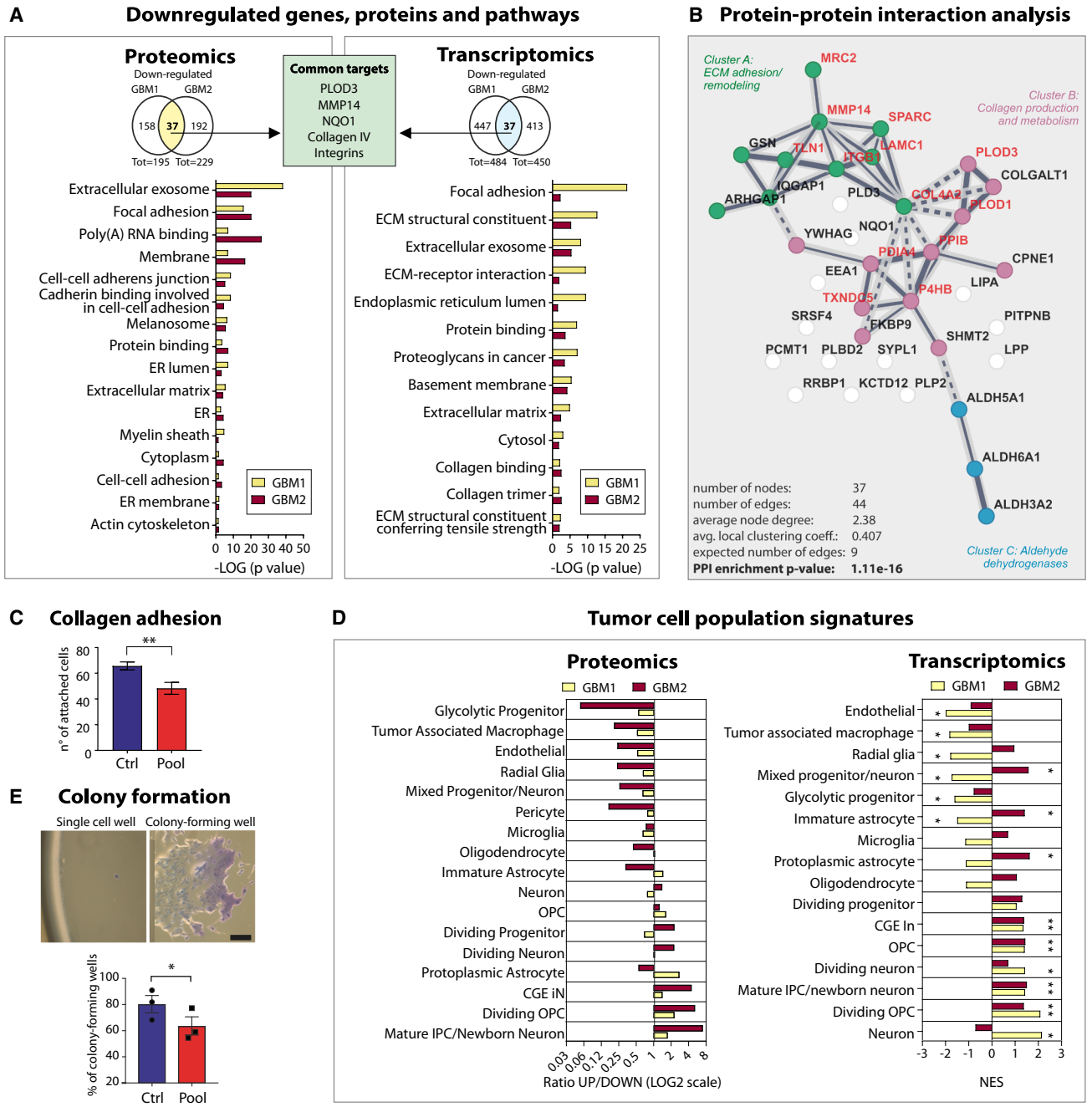

Figure 3. Multi-omics analysis, assessment of adhesion, and colony formation in GBM cultures after POOL rescue

(A) Proteomic and transcriptomic analysis of scrambled RNA and POOL-transfected GBM1, 2. *Top*, Venn diagram showing the number of proteins or genes downregulated by the POOL in each GBM (FDR <0.05) and the ones in common (LC-MS proteomics: $n = 5$ samples, 7 days after transfection; RNA-seq transcriptomics: $n = 3$ samples, 3 days after transfection). The green square highlights the common proteins/transcripts significantly downregulated by the POOL compared to control in both GBM1, 2. *Bottom*, pathway analysis (GO) of the 37 proteins downregulated by the POOL in both GBM cultures (for each GO term, the negative log of Benjamini-adjusted p value is plotted). (B) STRING protein-protein interaction (PPI) analysis of the 37 downregulated proteins in common between GBM1, 2. (C) Quantification of scrambled or POOL-transfected GBM2 cells attached on collagen IV-coated coverslips after 5 min of exposure ($n = 1$ experiment, in 5 replicates; two-tailed unpaired t test, $^{**}p < 0.005$). (D) Analysis of the relative enrichment of tumor cell population signatures (clusters as defined in Bhaduri et al.[2]) in proteomics and transcriptomics of GBM1, 2 upon POOL

(legend continued on next page)

(Figure 3A, *bottom*). Gene set enrichment analysis (GSEA) of transcriptomics data (Figure S3) highlights that "epithelial-mesenchymal transition" (EMT) was among the top downregulated pathways by the POOL in both GBMs, together with "tumor necrosis factor alpha signaling via nuclear factor κβ" and "transforming growth factor β signaling," two main inducers of EMT, and involved in GBM invasiveness and therapy resistance.[31] Notably, protein-protein interaction (PPI) analysis indicated a high degree of functional redundancy between the proteins downregulated by the POOL (Figure 3B), as indicated by their inclusion in a network with significantly enriched number of interactions. *k*-means analysis performed by STRING algorithm clustered the proteins into three main groups, whose functions can be summarized as the following: ECM adhesion and remodeling (*cluster A*), collagen production and metabolism (*cluster B*), and aldehyde dehydrogenases (*cluster C*) (Figure 3B). Interestingly, the latter family of enzymes is overexpressed in GBM and has been associated with therapy resistance, invasiveness, and stemness.[32] Among the downregulated transcripts/proteins/pathways, we noted an enrichment in ECM-interacting components and particularly collagen-related pathways: indeed, 13 of the 37 proteins (*names in red* in Figure 3B) are involved in collagen synthesis, post-translational modification, remodeling, recycling, or binding, suggesting that the POOL might inhibit tumor ability to synthesize and/or interact with this ECM component. In agreement, the POOL inhibited GBM2 cell adhesion (Figure 3C) on collagen and invasiveness of both GBM subtypes in this ECM (see Figure 2). This evidence indicates that the tumor-suppressive action of the POOL is primarily mediated by the modulation of cell-to-cell and cell-to-ECM adhesion, particularly by suppressing genes of the collagen pathway in both GBM subtypes.

To address whether the miRNA POOL modulates GSC subpopulations in the two GBMs, we classified the differentially expressed transcripts/proteins upon POOL transfection using clusters of GBM cell subpopulations from previous single-cell RNA-seq studies.[2,33] Interestingly, markers of GSC subpopulations (*glycolytic progenitor* and *radial glia*) and those associated to tumor-promoting features (*tumor-associated macrophages*) were less represented in both POOL-transfected GBM subtypes (Figure 3D).[3] The POOL also downregulated markers of vasculogenic potential of GSCs (*endothelial*, *pericyte*) (Figure 3D), which can transdifferentiate into vascular endothelial cells.[34] To ascertain whether the reduction in the abundance of stemness markers reflected a depletion of GSC subpopulation, we seeded individual POOL- or scramble-transfected cells and performed a clonogenic assay on Matrigel-coated coverslips by quantifying the generation of new colonies. Two weeks after POOL transfection, we found a significantly lower number of colony-forming wells, compared to scrambled control (Figure 3E). This result indicates that the POOL leads to a reduction of the GSC subpopulation.

Collectively, this evidence indicates that the POOL reduces invasiveness and stemness in GBM cultures and strongly suggests that the modulation of cell-to-cell and cell-to-ECM adhesion, particularly the downregulation of the collagen pathway, represents a common mechanism underlying the tumor-suppressive functions of the POOL in GBM of different subtypes.

Implementation of a synthetic nanocarrier for *in vivo* intratumor delivery of small RNAs in GBM

To implement a delivery strategy suitable for testing the POOL efficacy *in vivo*, we engineered a nanocarrier by encapsulating equimolar concentrations of the 11 miRNA mimics in lipid nanoparticles (LNPs) via microfluidic-based mixing (Figure 4A). Notably, a similar formulation has been approved by the US Food and Drug Administration to deliver small interfering (siRNA) to hepatocytes in the treatment of transthyretin amyloidosis.[35]

The charge of the 11 miRNAs was neutralized by ionizable lipids, mixed with neutral lipids and PEGylated lipids to generate particles of ∼120 nm diameter (Figure 4B). To overcome the low uptake of uncoated LNPs by cancer cells, apolipoprotein E (ApoE, Figure 4A), which is the ligand of the lipoprotein receptor overexpressed in several cancer cell types including GBM, was adsorbed on the surface of the nanoparticles.[36,37] Cryo-electron microscopy characterization of the LNPs showed a multi-lamellar structure (Figure 4B), in line with previous reports for similar particles. The LNP and ApoE-LNP hydrodynamic diameters were 127 and 135 nm, respectively (*bars* in Figure 4C). A low polydispersity index (PdI) was observed (*dotted lines* in Figure 4C), indicating a homogenous size distribution of the particles for both preparations. To ascertain the coating of ApoE, we measured the zeta potential of the LNPs. As expected, the zeta potential of ApoE-LNPs was negative compared to uncoated LNPs and thus consistent with the negative charge of this protein (Figure S4).

To test whether the nanocarriers could deliver miRNAs into GBM cells *in vitro*, we loaded FAM-labeled siRNA (same size of miRNA mimics) into LNPs with or without ApoE coating and administered them to a GBM cell line (U87MG). As a positive control, we transfected the same siRNA with Lipofectamine. As expected, FAM-labeled siRNA loaded into LNPs was not efficiently taken up by the cells as indicated by flow cytometry analysis at both 2 and 5 h after cell treatment (Figure 4D). Conversely, FAM-labeled siRNAs were successfully taken up by the cells when loaded into ApoE-coated LNPs, even more efficiently than with Lipofectamine, at both time points after treatment (Figure 4D). Confocal imaging of GBM cell line treated with ApoE-LNPs confirmed the intracellular localization of FAM-labeled siRNA (Figure S4).

transfection. Proteomics: ratio of the number of up- to downregulated proteins from each cluster (ratio <1: downregulated by the POOL). Transcriptomics: normalized enrichment score (NES) of each cluster obtained from GSEA analysis of POOL- versus control-transfected GBM (NES <0: downregulated by the POOL; *FDR q value < 0.005). (E) Quantification of colony-positive wells 2 weeks after seeding single cells of POOL- or scrambled control-transfected GBM2 cultures, relative to the number of colony-positive wells of untransfected GBM cells (n = 3 independent experiments, at least 30 wells/condition; two-tailed, paired t test; *$p < 0.05$). Scale bar, 100 μm.

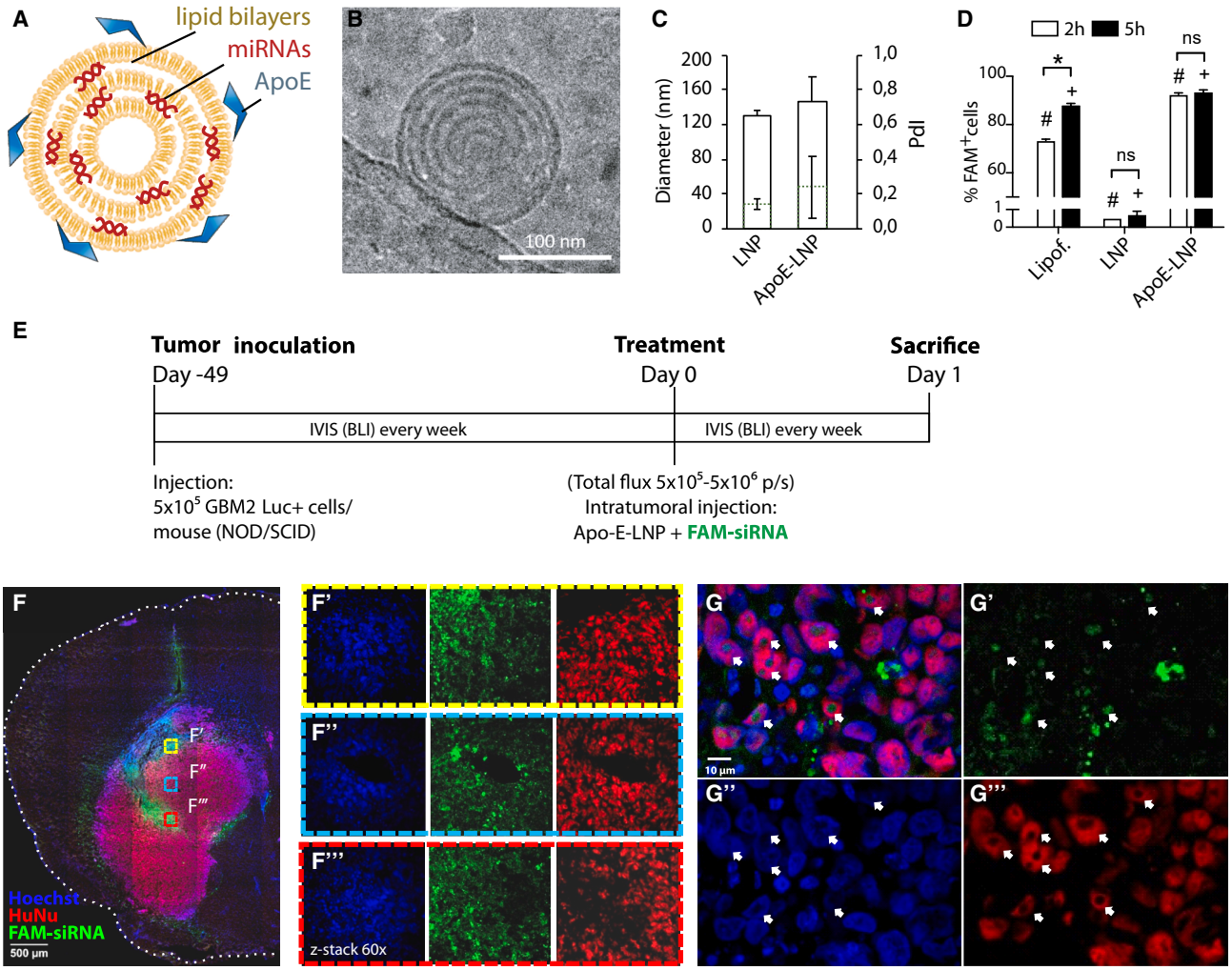

Figure 4. *In vitro* characterization of the nanocarrier and *in vivo* biodistribution of the small RNA cargos upon intratumor injection in a preclinical mouse model with orthotopic GBM xenotransplants

(A) Scheme of the ApoE-LNP nanocarrier. (B) Cryo-electron microscopy showing one representative image of LNP. (C) Diameter (*bars*) and polydispersity index (PdI, *dotted lines*) measurement of LNP with or without ApoE coating (mean ± SD of at least 4 independent batches measurements). (D) Percentage of U87MG cells positive for the FAM-labeled siRNA fluorescence 2 or 5 h upon Lipofectamine 2000 (positive control), LNP, or ApoE-LNP incubation, as determined by flow cytometry ($n = 2$ replicates) (# and + mark conditions statistically different among them; two-way ANOVA and multiple comparisons; *$p < 0.05$). (E) Experimental scheme of GBM2 orthotopic xenotransplantation in NOD/SCID mice and intratumor injection of ApoE-LNP loaded with FAM-siRNA. (F) Representative images of FAM-siRNA (green) distribution in the tumor mass (Hoechst, *blue*; FAM-siRNA, *green*; Human Nuclei, HuNu, *red*; objective 10×; scale bars, 500 µm) 24 h after intratumor injection of FAM-siRNA-loaded ApoE-LNPs. (F′–F‴) Higher magnification showing the distribution of the three signals inside the tumor mass (indicated by the boxed regions in F; z stack 60×). Note that the green signal intensity is similar between the three tumor areas at different distances from the injection site/tumor mass center. (G) Confocal images showing merged (G) and separate channels (G′–G‴) of FAM-siRNA (green) inside the human GBM cells (HuNu, *red*; Hoechst, *blue*). Note that GBM cells appear bigger than the (HuNu-negative) mouse cells. Objective 60×; scale bars, 10 µm.

To test the toxicity *in vivo*, we injected the nanoformulated FAM-labeled siRNA in the brain of healthy mice, and no tissue damage or cell death was observed in the area surrounding the injection (*data not shown*), in agreement with the known low neurotoxicity of ApoE-LNPs.[38] To test the biodistribution and the intracellular delivery of miRNAs via ApoE-LNPs, we implemented a xenotransplant mouse model by orthotopic injection of human GBM cells (i.e., GBM2) constitutively expressing the luminescent reporter luciferase (Luc^+) in the striatum of NOD-SCID mice. Tumor formation and growth were monitored for the subsequent 49 days by the IVIS spectrum *in vivo* imaging system. FAM-labeled siRNAs loaded in ApoE-LNPs were injected intratumorally, and brains were harvested 24 h after injection for histological analyses (Figure 4E). Fluorescence confocal microscopy imaging of immunostained sections across the brain of NOD-SCID mice showed FAM fluorescence (Figure 4F, *green*) uniformly distributed in several regions of the engrafted tumor, identified

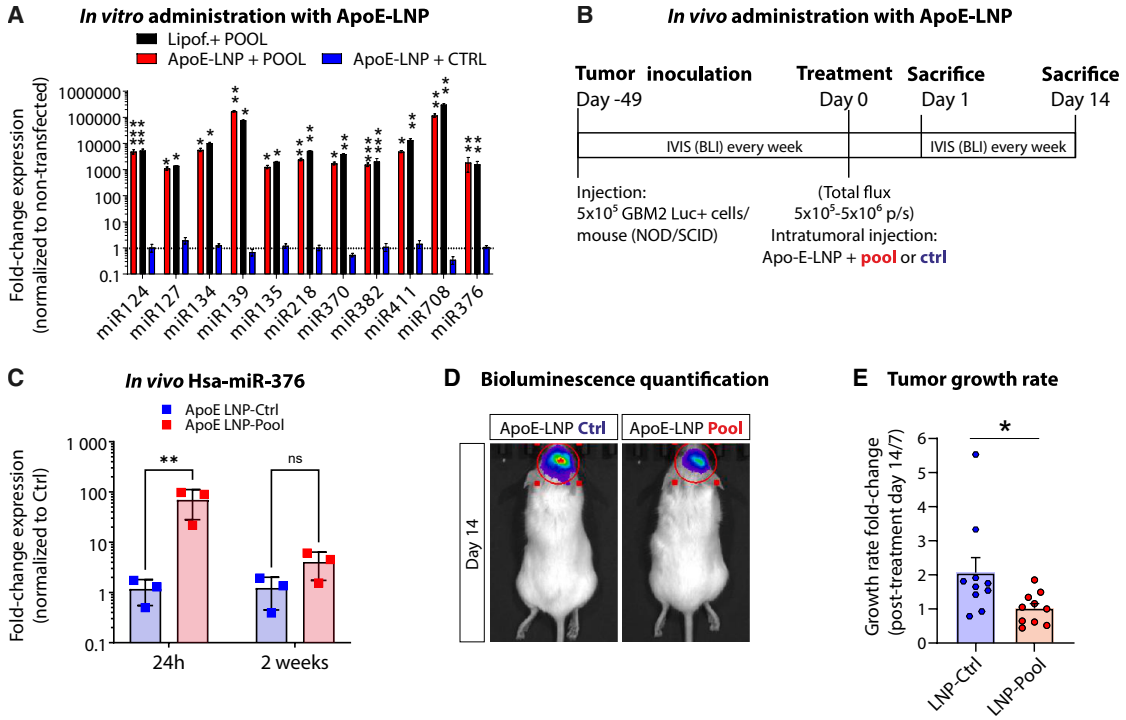

Figure 5. *In vivo* stability and therapeutic efficacy of the miRNAs upon a single intratumor injection of nanoformulated POOL

(A) Real-time qPCR-mediated quantification of the 11 miRNAs levels 5 h after *in vitro* delivery of the POOL with Lipofectamine, or POOL- or scrambled control (ctrl)-loaded LNPs, coated or uncoated with ApoE (data are expressed as fold-change expression and normalized to untreated condition; ΔΔct mean ± SD; ApoE-LNP samples are $n = 2$ biological replicates, real-time qPCR samples are analyzed in technical triplicate; one-way ANOVA and multiple comparison, $^{*}p < 0.05$, $^{**}p < 0.01$, $^{***}p < 0.005$). (B) Experimental scheme of the *in vivo* xenotransplantation and intratumor injection of the nanoformulated POOL. (C) Levels of hsa-miR376b in xenotransplanted GBM after intratumor injection of nanoformulated POOL or scrambled RNA ($n = 3$ animals per condition; $^{**}p < 0.005$, two-way ANOVA and multiple comparisons). (D) Representative images of xenotransplanted mice 14 days after intratumor injection of nanoformulated POOL or scrambled RNA as assessed by IVIS bioluminescence. (E) Tumor growth rate represented as ratio of the total flux (p/s) as assessed by IVIS bioluminescence at day 14/day 7 upon intratumor injection of the nanoformulated POOL or scrambled RNA ($n =$ 10 animals; data are the mean ± SEM; $^{*}p = 0.03$, unpaired two-tailed *t* test).

by the positivity for the human-specific nuclear antigen HuNu (Figure 4F, *red*). Higher magnification of the engrafted tumors confirmed the intracellular delivery of the FAM-labeled siRNAs in human GBM cells (Figure 4G). Hence, a single injection of the nanoformulation allows efficient intratumor distribution and intracellular delivery of a synthetic siRNA in human GBM *in vivo*.

A single intratumor administration of the nanoformulated POOL reduces GBM progression *in vivo*

To test whether the ApoE-LNPs could simultaneously deliver the 11 miRNAs to GBM cells, we loaded either the 11 miRNAs or the scrambled RNA in the ApoE-LNPs. The encapsulation efficiency was 79.5% ± 5.3% for the miRNA POOL and 86.3% ± 2.0% for the scrambled. Real-time qPCR of GBM2 cultures treated with POOL-loaded ApoE-LNPs confirmed the rescue of the expression of all the 11 miRNAs, compared to cells treated with scrambled RNA-loaded ApoE-LNPs, with the same efficiency of Lipofectamine (Figure 5A).

To assess the phenotypic effect of the nanoformulated POOL in the preclinical model of GBM xenotransplantation *in vivo*, 42–49 days after implantation of Luc^{+} GBM2 cells in the striatum of NOD/SCID mice, we injected intratumorally POOL- or scramble-loaded ApoE-LNPs. Growth of GBM tumor xenografts was monitored for 2 weeks after injection of the nanoformulated RNAs by IVIS-mediated quantification of luciferase signal, and brains were harvested for further analyses (Figures 5B–5D). *In vivo* stability of the nanoformulated POOL was assessed by quantifying levels of the hsa-miR-376b-3p, the only human-specific miRNA of the POOL (Table S1). Human miR-376b-3p, which bears a difference of 3 nucleotides compared with the mouse homolog, was used to design a human-specific real-time qPCR assay to distinguish the injected miR from the endogenous one (Figure S5). Hsa-miR-376b-3p levels were significantly increased in the GBM tumor 24 h after local injection of the ApoE-LNPs loaded with the POOL, compared to GBM injected with control ApoE-LNPs (Figure 5C). However, at 14 days post injection, levels of the hsa-miR-376b-3p returned to almost basal (Figure 5C). Assuming similar kinetics for all the miRNAs of the POOL, this result suggests that the nanoformulated miRNAs are stable for less than 2 weeks after intratumor injection *in vivo*.

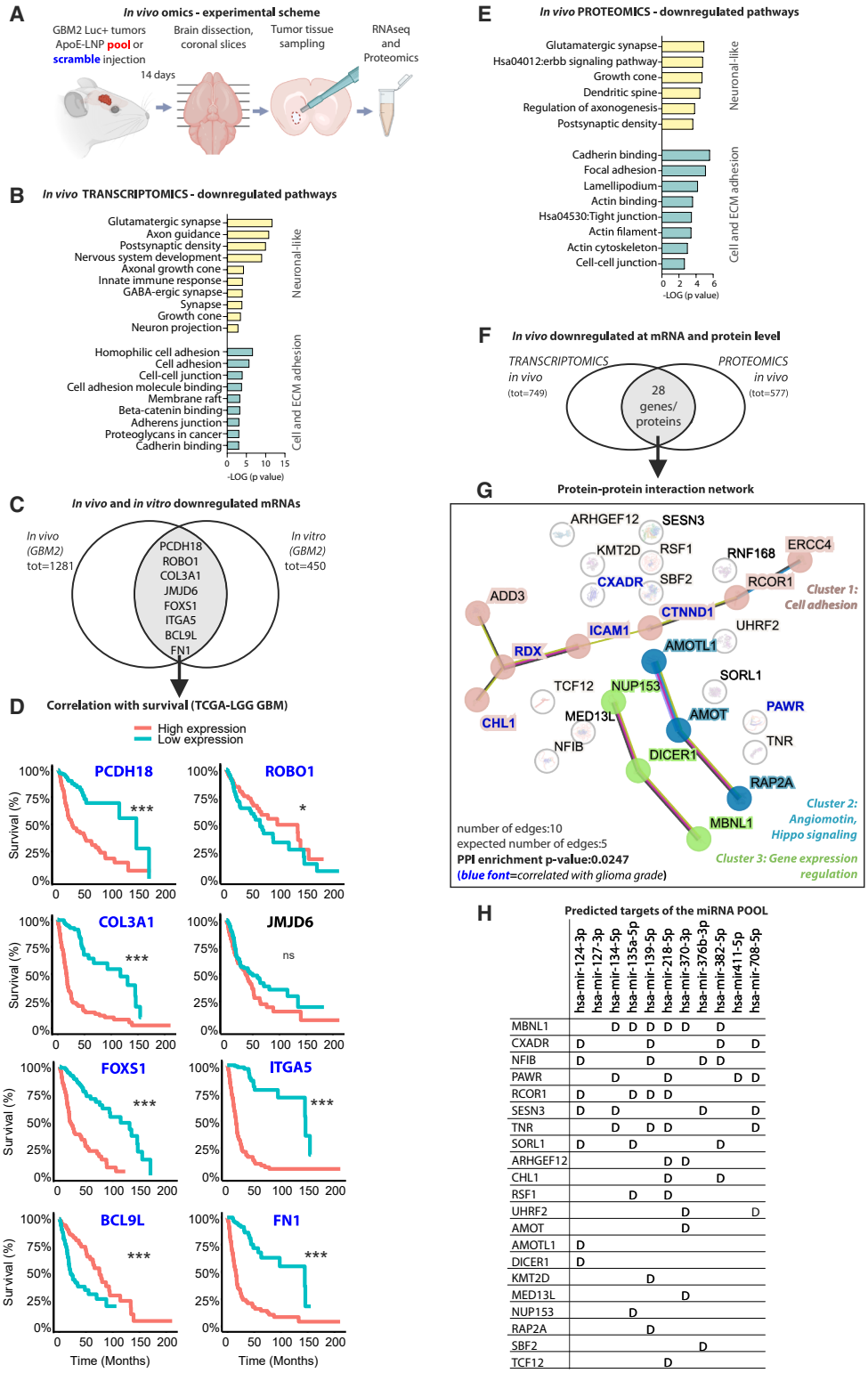

	hsa-mir-124-3p	hsa-mir-127-3p	hsa-mir-134-5p	hsa-mir-135a-5p	hsa-mir-139-5p	hsa-mir-218-5p	hsa-mir-370-3p	hsa-mir-376b-3p	hsa-mir-382-5p	hsa-mir411-5p	hsa-mir-708-5p
MBNL1			D	D	D	D	D		D		
CXADR	D				D				D		D
NFIB	D				D			D	D		
PAWR			D			D				D	D
RCOR1	D			D	D	D					
SESN3	D		D					D			D
TNR			D		D	D					D
SORL1	D			D					D		
ARHGEF12						D	D				
CHL1						D			D		
RSF1				D		D					
UHRF2								D			D
AMOT								D			
AMOTL1	D										
DICER1	D										
KMT2D					D						
MED13L								D			
NUP153				D							
RAP2A					D						
SBF2									D		
TCF12							D				

(legend on next page)

Remarkably, a single injection of the ApoE-LNP POOL significantly inhibited the rate of GBM growth for 2 weeks following the treatment, compared to the group of mice injected with scrambled-loaded ApoE-LNPs (Figures 5D and 5E), after which the growth rate of POOL-injected tumors returned to levels comparable to the control group (*not shown*), in line with the observed stability of the miRNA mimics *in vivo*. This result confirms the tumor-suppressive efficacy of the POOL in a preclinical model of human GBM.

Clinically relevant targets underlie the tumor-suppressive functions of the POOL *in vivo*

To validate the mechanisms underlying the efficacy of the POOL in xenotransplanted GBM, 2 weeks after intratumor injection of POOL- or scramble-loaded ApoE-LNPs, we performed transcriptomics and proteomics on tumor tissue samples (Figure 6A; Tables S6 and S7) and focused on the human transcripts and proteins downregulated *in vivo*. To this end, we filtered out mouse-specific entries from the omics data, as detailed in the materials and methods section.

Pathway analysis of transcripts downregulated upon POOL administration *in vivo* (Figure 6B) confirmed cell- and ECM-adhesion pathways, largely overlapping with the ones from *in vitro* transcriptomics. Concomitantly, this analysis revealed several neuronal and neuro-developmental GO terms downregulated upon POOL administration *in vivo* (Figure 6B). Indeed, neural-specific pathways and synaptic genes have been associated to GBM infiltration by several reports, in line with the fact that GSCs hijack the neuronal genetic programs to invade the brain parenchyma.[39,40] These results confirm that repression of the tumor-ECM interaction and EMT-related pathways underlies the tumor-suppressive functions of the miRNA POOL in GBM *in vivo*. Moreover, eight downregulated genes were in common between *in vivo* and *in vitro* transcriptomics (Figure 6C). Notably, five of them encode proteins involved in cell adhesion, motility, or ECM interaction in GBM or other cancer types (i.e., *PCDH18*, *COL3A1*, *ITGA5*, *FN1*, and *ROBO1*), and the other three encode either transcriptional or epigenetic regulators involved in EMT (i.e., *FOXS1*), stemness (*BCL9L*), or GBM growth (i.e., *JMJD6*), respectively.[41–48] We also investigated miRNA-mRNA interaction databases and found that the majority (six out of eight) of the repressed genes (*Venn diagram* in Figure 6C) are predicted or validated targets of one or more miRNAs from the POOL (Table S5). To understand the clinical relevance of the eight genes suppressed by the POOL in GBM, we retrieved clinical information from the TCGA-LGG GBM database. Interestingly, the expression of seven out of eight genes positively correlates with reduced survival in patients (Figure 6D), in line with previous reports in GBM, and six of them positively correlate with glioma grade (Figure S6; Table S8), being significantly overexpressed in GBM compared to grade II and III gliomas.[41–44]

Pathway analysis performed on the downregulated proteins *in vivo* substantially confirmed that the POOL primarily affects neuronal-like and cell-ECM interaction pathways (Figure 6E). By comparing transcriptomics and proteomics, we identified 28 terms that were downregulated *in vivo* by the POOL at both transcript and protein levels (Figure 6F). This group of proteins is functionally interconnected and involved, as indicated by *k*-means clustering, in cell adhesion (CTNND1, ADD3, RDX, and ICAM1) and neuron-specific differentiation programs (CHL1 and RCOR1) (Figure 6G; Table S9). Interestingly, six of these proteins correlate with glioma grade (Figure S6; Table S8), and 13 have been previously reported to exert a tumor-promoting function in GBM (Table S9). Finally, we checked the miRNA-target interaction databases and found that most of the 28 transcripts are predicted targets of at least one miRNA of the POOL, with 12 of them having more than two predicted interactions (Figure 6H).

These results confirm that the POOL represses key genes involved in mechanisms that are aberrantly upregulated in GBM, highlighting new targets suitable for future diagnostic and therapeutic developments.

DISCUSSION

This study highlights the synergistic potential of pro-neural miRNAs as a multimodal therapeutic strategy for GBM, one of the most lethal cancers in humans. We restored the expression of 11 miRNAs that are underexpressed in gliomas and likely involved in GBM initiation and progression. Our results show that this miRNA cocktail significantly reduces GBM growth, invasion, and stemness in both *in vitro* and *in vivo* models. A single intratumor injection of the nanoformulated miRNA POOL significantly slowed human GBM progression

Figure 6. Genes, pathways, and targets suppressed by the POOL *in vivo* are prognostically relevant in GBM patients

(A) Experimental scheme of the experiment for *in vivo* transcriptomics and proteomics. (B) *In vivo* transcriptomics: pathway analysis (GO enrichment) of transcripts downregulated by the POOL. The most statistically significant GO terms and KEGG (indicated by the code "Hsa") pathways are grouped in two clusters, related to nervous system cell development and morphology (in *yellow*) and cell-/ECM-adhesion (in *blue*). Only terms with FDR <0.05 were selected, negative log of *p* value is plotted. (C) Venn diagram showing transcripts downregulated in GBM2 both *in vitro* and *in vivo* upon POOL administration. (D) Correlation between expression of the 8 transcripts from (C) and patients' survival: Kaplan-Meier curves from TCGA-LGG GBM patients dataset (cutoff: high vs. low, log rank *p* value: ***<0.001, *<0.05, in *blue*: statistically significant. Statistics in Table S8). (E) *In vivo* proteomics: pathway analysis (GO enrichment) of proteins downregulated *in vivo* 2 weeks after POOL administration (selected pathways are plotted similarly as in B, as they can be grouped in the same two clusters). (F) Venn diagram showing that 28 protein-coding genes are significantly downregulated *in vivo* by the POOL at both protein and transcript level. (G) STRING protein-protein interaction network for the 28 terms in (F). In *black*, *bold font*: proteins belonging to one of the 3 identified clusters (*k*-means analysis, STRING); in *blue*, *bold font:* proteins whose expression (at transcript level) was found to inversely correlate with glioma grade (TCGA-LGG GBM dataset, Gliovis analysis, see Figure S6; Table S8). (H) Results of miRNA target prediction analysis for the 28 downregulated genes and the 11 miRNAs (DIANA-microT, combining miRBase 22.1 and MirGeneDB 2.1 databases; only mRNAs with at least one predicted miRNA-target interaction are plotted, indicated with a "D").

in the preclinical model. Hence, this study successfully addresses relevant problems underlying the poor prognosis of GBM patients.

Based on the existing literature, this study is the first to demonstrate the efficacy of a "fully synthetic" formulation of different miRNAs to treat GBM *in vivo*. Unsurprisingly, the effects were transient in line with the synthetic nature of the formulation. Hence, we anticipate that multiple rounds of local administration will likely be required to improve animal survival rate. Intratumor injection of synthetic formulations of small RNAs is feasible in the clinical setting and may offer several advantages, including a potentially faster approval process compared to viral and/or cell-based vectors.[15,49] Future studies should explore alternative delivery methods, such as biodegradable implants, or chemical modifications of the mimics to enhance stability of the miRNAs to prolong therapeutic effects.[50,51]

As related to the translational value of the miRNA synergism as a multimodal gene therapy, recent publications have convincingly demonstrated that restoring combinations of different miRNAs significantly improves anticancer efficacy compared to a single miRNA.[13,17–21] However, so far, polycistronic transcripts bearing different precursors were typically used to express combinations of miRNAs in GBM.[19,20] This strategy still poses some challenges that complicate their clinical translation. Indeed, it does not guarantee constant transcription of the polycistronic precursor, nor the equimolar expression of the different miRNAs in the tumor. Moreover, cleavage of hairpin miRNAs from polycistronic precursors and miRNA maturation rely on endogenous biogenesis proteins such as Drosha and Dicer, often dysregulated in cancer.[52] Furthermore, when the polycistronic precursor is delivered by viruses, the tropism of this carrier may not allow equal targeting of the different cell subpopulations in GBM. Additionally, viral carriers may trigger immune responses, complicating their repeated administrations. While some of the limitations related to the viral transduction have been recently overcome by using exosomes as carriers, this approach relies on a plasmid-encoded polycistronic precursor to express multiple miRNAs, which may still suffer from the limitations of such constructs discussed earlier.[20] Nonetheless, the path to the therapeutic use of multiple miRNAs for GBM is now wide open, and we are confident that one of the promising RNA delivery strategies currently in trials will soon be pivotal in translating the miRNA synergism approach in neuro-oncology.[17]

At the functional level, the multi-omics analysis indicates that the POOL represses the collagen pathway and suggests that this may contribute to reducing the GSC niche, providing a mechanistic framework for the tumor-suppressive effects of these miRNAs. This is in line with the reduced adhesion and invasiveness of GBM cells upon POOL rescue. Indeed, collagen is a crucial component of the basement membrane, the brain-specific ECM that surrounds blood vessels, a microenvironment that provides means to both GSC niche maintenance and GBM cell migration. In fact, GBM cells invade through the brain parenchyma along the vessels, and the ability of malignant cells to interact with collagen is a crucial determinant of invasiveness and maintenance of the stem cell niche.[53] The precise cascade of events underlying the efficacy of the POOL against the GSC subpopulation warrants further studies. Nonetheless, our results align with the notion that modulation of genes involved in ECM organization, cell-ECM adhesion, and promotion of cell migration occurs in GSCs as they transition toward "differentiated" glioma cells.[54]

Finally, despite the inherent heterogeneity of GBM, we identified key genes and pathways to inhibit tumor progression. Because these genes positively correlate with poor prognosis and higher glioma grades in patients, we are confident that they have the potential to serve as targets for future therapies and diagnostic development.

MATERIALS AND METHODS

Cell cultures and *in vitro* assays

High-grade primary GBM cells (tumor ID GBM1: GSC#Ge003 1740R-48-11; tumor ID GBM2: GSC#Ge023 1740R-48-17; GG3: GBM5 from Griffero et al.[27]) were established and cultured as previously described.[27,30] U87MG cells (from ATCC) were grown as monolayer in EMEM supplemented with 2 mM L-glutamine and 10% fetal bovine serum (Gibco).

Transfection

Lipofectamine2000 (Life Technologies) was used to transfect the miRNA POOL (25 nM of each miRNA mimic) or scrambled siRNA as control (miRIDIAN, Dharmacon); in each subPOOLs of 10 miRNAs, the missing miRNA was compensated by 25 nM of scrambled RNA, to maintain equal final concentrations.

Migration/invasion assay

After 24 h transfection, 30,000 cells/well were seeded in Matrigel-coated ImageLock (Sartorius) 96-well plates; after additional 24 h, the scratch was produced with a wound maker (Sartorius). Cells were kept in complete medium (migration assay) or coated with a layer of diluted Matrigel (Corning, 1:40 in DMEM, Gibco) and let in the incubator for 20 min before adding complete medium (invasion assay).

Cell growth

After 24 h transfection, 5,000 cells/well were plated in Matrigel-coated 96-well plates and imaged for 72 h with Incucyte (Sartorius) using phase confluence mask analysis to obtain confluence normalized on time zero. TMZ powder (Merck) was dissolved in DMSO (100 mM stock) and diluted in complete medium to a concentration of 1,500 μM. From this, serial dilutions (1:2) in complete medium were prepared to the indicated range of concentrations.

3D cultures in collagen hydrogels

After 24 h transfection, 500 cells/well were seeded in an ultra-low attachment 96-well plate (InSphero) for 24 h. Spheroids were transferred into collagen type I hydrogels and cultured for 7 days. Hydrogel preparation: collagen type I solution (3 mg/mL, Sigma-Aldrich) was mixed with a phosphate-buffered

saline (PBS), EMEM (5×) with phenol red, 0.1 M NaOH, and sterile water to yield a final collagen concentration of 2 mg/mL at pH of 7.4.

Cell adhesion on collagen

5,000 cells/coverslip of control- or POOL-transfected GBM cells were seeded 72 h after transfection on glass coverslips pre-coated with human collagen IV (Corning; 10 mg/mL) and left to adhere for 5 min; then, they were washed and cultured for 2 h in fresh medium, fixed with 4% paraformaldehyde (PFA), stained with Hoechst (1:1.000), and counted.

Clonogenic assay

GBM cells were transfected as indicated earlier. 24 h after transfection, single cells were seeded in Matrigel-coated 96-well plates, and colonies were imaged under a transmitted light microscope for 2 weeks with a 10× objective in an Olympus CKX41 inverted microscope. The colony-forming wells were counted and normalized on colony-forming wells of non-transfected condition.

Flow cytometry

U87MG cells were seeded at 8×10^4 cells/well on 24-well plates. After 24 h, cells were treated with FAM-loaded LNPs (100 nM final FAM-RNA concentration) in complete medium. Transfection of FAM-RNA (MISSION siRNA, Merck) was used as a positive control as described earlier. Cells were analyzed with a FACs aria IIIu cytofluorometer in PBS 2 and 5 h after LNP treatment.

Imaging

Live-cell imaging

Cultured cells were imaged with Incucyte (Sartorius) and analyzed with Scratch Wound software module, using relative wound density (%) and wound confluence (%) parameters to quantify invasion and migration, respectively, as recommended by the vendor.

Bright-field imaging

3D spheroids in hydrogel were imaged with a 5× objective in a Leica DMI6000 inverted microscope. Spheroid core area was quantified with Fiji ImageJ software, and the relative radius is calculated; the external perimeter formed by spheroid protrusions was selected, and the spheroid core area was subtracted to obtain the invasion area of each spheroid.

Fluorescence imaging (in vivo biodistribution)

A 10× objective of a microscope Olympus BX51 equipped with the Neurolucida stage and software (MBF Bioscience) was used to acquire an overall visualization of tumor cells (stained with HuNu) in the striatum and the distribution of FAM-labeled siRNAs (green signal) inside the tumor mass. Then, five images were captured around the injection site of FAM-labeled siRNAs with Nikon A1 confocal microscope at 40× objective, and finally, some images were taken with 60× objective to observe the localization of FAM-labeled siRNAs inside the tumor cells at higher resolution.

IVIS imaging

To evaluate tumor growth *in vivo*, D-luciferin potassium salt (150 mg/kg, PerkinElmer) was intraperitoneally injected into all mice, 10 min after animals were anesthetized and *in vivo* bioluminescence imaging of the tumor growth was captured using the IVIS Spectrum Imaging System (PerkinElmer). Regions of interest were defined using Living Image software, and total photon flux (p/s) was quantified once a week.

LNPs

Microfluidics

Nanoassemblr (Precision NanoSystems) was used to mix one volume of 1,2-dioleoyl-3-dimethylammonium-propane (DODAP), 1,2-dipalmitoyl-sn-glycero-3-phosphocholine (DPPC), 1,2-distearoyl-sn-glycero-3-phosphoethanolamine-*N*-[methoxy(polyethylene glycol)-2000] (DSPE-PEG2k) (Avanti Polar Lipids, Inc.), and cholesterol (Merck) in ethanol (DODAP, DPPC, cholesterol, and DSPE-PEG2k at 50/10/38.5/1.5 mol ratio) with 4 volumes of citrate buffer (pH 3.9, 50 mM) containing the miRNAs or scramble RNA (Dharmacon) or an FAM-labeled siRNA (Merck) at the final lipid/RNA ratio of 39:1 (w/w), for the *in vitro* formulation, or 20:1 (w/w) for the *in vivo* one. Total flow rate was 2 mL/min. LNPs were dialyzed for 16–20 h against 500× volume of PBS pH 7.4 and then sterilized through 0.22 μm PVDF syringe filters (Millipore). For *in vivo* experiments, LNPs were concentrated by centrifugal ultrafiltration units (Amicon Ultra 4, 30 kDa MWCO, Millipore).

LNP coating with ApoE3

1 mg of human ApoE3 peptide (PeproTech) per 140 mg lipids was incubated for 5 min at 37°C. To summarize, the calculated concentrations of components in the final product for the *in vitro* formulation were as follows: DODAP (2.20 mg/mL), DPPC (0.50 mg/mL), cholesterol (1.01 mg/mL), DSPE-PEG2k (0.285 mg/mL), miRNA POOL (0.102 mg/mL), and ApoE (0.0286 mg/mL); and for the *in vivo* formulation were: DODAP (68.75 mg/mL), DPPC (15.62 mg/mL), cholesterol (31.56 mg/mL), DSPE-PEG2k (8.906 mg/mL), miRNA POOL (6.3 mg/mL), and ApoE (0.892 mg/mL).

Characterization

Diameter, PdI, and z-potential of LNPs were measured using a Nano-ZS Zetasizer (Malvern) in deionized water.

RNA encapsulation efficiency was determined by Ribogreen assay (Thermo Fisher Scientific) following the manufacturer protocol, with a plate reader (Tecan) before and after the lysis of LNPs with Triton X (0.5% w/w). *Cryo-electron microscopy* of LNPs was done with FEI Tecnai G2-F20.

LNP in vitro transfection efficiency

U87MG cells (5 × 104 cells/well) were seeded into eight-chambered cover glass system for confocal imaging (Lab Tek II, Thermo Scientific) or 8×10^4/well in multiwell-24 for flow cytometry analysis and kept in complete medium for 24 h. Cells were then treated with LNPs loaded with either FAM-labeled

siRNA (final siRNA concentration, 100 nM) for 2 or 5 h and then either fixed with 4% PFA and stained with WGA and DAPI for imaging or analyzed with a BD-FACS aria III cytofluorometer. Real-time qPCR: PD-GBM (8×10^4/well) were seeded in multiwell-24 and kept in complete medium for 24 h and then treated for 5 h with LNP loaded with either miRNA mimics or scrambled RNA (final concentration was 25 nM of each miRNA mimic and 250 nM of scrambled RNA).

Animal procedures

All care of animals and experimental procedures were conducted in accordance with IIT Animal Use Committee and were approved by the Italian Ministry of Health. NOD/SCID female mice (Charles River, Italy) were group housed in ventilated cages in a climate-controlled animal facility (22°C ± 2°C) and maintained on a 12 h light/dark cycle with *ad libitum* access to food and water. Surgery: anesthetized animals (2% isoflurane/0.8% oxygen) were operated with a stereotaxic apparatus keeping them on a warming pad at 37°C. 3 μL of suspension containing 5×10^5 human GBM cells (GBM2-Luc+) were injected into the striatum (coordinates, AP: 1; ML: −2; DV: −3 from bregma) by a syringe (Hamilton) connected to a pump, skin was sutured with absorbable wire, and mice were monitored until recovery.

Intratumor injection of nanoformulated miRNAs

Around 42–49 days after xenotransplantation (i.e., when the rate of tumor growth started to rise, as quantified by IVIS), 3 μL of ApoE-LNPs loaded with FAM-labeled siRNAs, or POOL or scramble RNA (corresponding to 1.35 nmol of RNA) was injected into each animal. The site of injection and procedure were the same as those used for GBM cell implantation.

Histology

About 24 h after injection of FAM-labeled siRNAs loaded into ApoE-LNPs, mice were anesthetized with a mixture of xylazine/ketamine (intraperitoneally) and perfused with cold PBS at pH 7.4 and then with 4% PFA in PBS. Brains were post-fixed in PFA overnight at 4°C and then put in 30% sucrose for 2 days, then frozen in isopentane solution and stored at −80°C. 30-μm-thick brain sections were cut on a cryostat, processed for antigen retrieval (10 min at 85°C in the oven with 100 mM citric acid at pH 6.0), preincubated for 1 h in blocking buffer (5% normal goat serum, 0.1% Triton X-100 in PBS), and incubated overnight at 4°C with primary antibodies mouse anti-Human Nuclear-Cy3 conjugated (MAB1281, Sigma, 1:100) to label human GBM2 cells. After washing, Hoechst nuclear staining was added (1:300), and the sections were mounted with Vectashield antifade mounting without DAPI (Vector Laboratories).

RNA-seq and qPCR

RNA isolation and extraction for qPCR were performed with TRIzol (Invitrogen) following manufacturer's instructions. Reverse transcription and SYBR green-based qPCR for miRNA were performed with miScript II RT kit and primers (QIAGEN); human U6 was used as housekeeping gene.

Transcriptomics (poly A)

After transfection with the POOL or scrambled RNA ($n = 3$ samples, per group), GBM cells were seeded at 80,000 cells/well in multiwell-24 plates and kept in non-adherent conditions (i.e., in complete medium without Matrigel coating, to allow spheroid formation) and then processed for RNA extraction using RNeasy kit (QIAGEN).

In vivo *transcriptomics*

GBM xenotransplanted mice were sacrificed 2 weeks after intratumor injection of POOL- or scramble-loaded ApoE-LNP (see animal procedures). Brains were harvested and cut with a slicer matrix kept on ice; 2 mm coronal slices were visually inspected, and tumoral tissue was withdrawn with brain punches (Integra LifeSciences) and fresh frozen. Tissue was lysed in RNA extraction buffer (RNeasy kit, QIAGEN), homogenized by sonication, and processed for RNA extraction (RNeasy kit, QIAGEN). RNA quality was assessed with Bioanalyzer (Agilent). 100 ng of RNA per sample was used to prepare libraries (Illumina Stranded mRNA Prep) and sequenced with a NovaSeq 6000 (Illumina).

Small RNA-seq

RNA was extracted with TRIzol, and 1 μg of RNA for each sample was used for library preparation with Nextflex Small RNA-Seq Kit (PerkinElmer, #NOVA-5132-06) with the following modifications: an amplification step on the fragments was carried out with 18 PCR cycles. The quality of the library was assessed by high-sensitivity DNA kit (Agilent, 5067-4626), and bidirectional sequencing was performed with NovaSeq 6000 using a flow cell Reagent Kit v.1.5 (Illumina, 20028401). As control, a human postmortem cerebellum and prefrontal cortex small RNA dataset were used (BioProject PRJNA752352, accession number: GSE181520).[26]

LC-MS proteomics

In vitro sample preparation: GBM1 and GBM2 were cultured and transfected as described earlier; 24 h after transfection, cells were detached and seeded at 80,000 cells/well in multiwell-24 plates, in non-adherent condition for 6 days. Protein extracts were prepared with ice-cold RIPA buffer containing protease inhibitors (Complete mini EDTA-free, Roche) and sodium orthovanadate (phosphatase inhibitor). Protein lysates were kept in agitation for 30 min, collected by centrifugation at 13,000 × *g* for 30 min at 4°C, and then stored at −80°C. 50 μg of proteins (quantified using the colorimetric Bradford dye-binding method, Bio-Rad kit) per sample was reduced with dithiothreitol (100 mM DTT in 50 mM NH_4HCO_3) at 56°C for 30 min, alkylated in 100 mM IAA in 50 mM NH_4HCO_3 (30 min at room temperature in the dark), and then precipitated with cold acetone (−20°C), overnight. Samples were then centrifuged (14,000 × *g* for 30 min at 4°C); the pellets were dried under nitrogen stream and resuspended in digestion buffer (50 mM NH_4HCO_3). Protein digestion into peptides was obtained by adding 0.5 μg/mL trypsin and incubating overnight at 37°C. A desalting procedure was conducted with Pierce C18 Spin columns; peptides were then dried and redissolved in 3% acetonitrile with 0.1% formic acid.

LC-MS analysis

The volume corresponding to 1.65 μg of peptides was injected on a NanoAcquity chromatographic system. The chromatographic method was set as follows: for the trapping phase, an Acquity C18 column (180 μm × 20 mm, from Waters, Milford, MA, USA) was used, and the peptides were loaded at 4.0 μL/min (1% acetonitrile + 0.1% FA) for 4 min; the peptides were then moved into a PicoFrit C18 column (75 μm × 25 cm, NewObjective Inc.) and eluted at 300 nL/min with a 2 h gradient of acetonitrile in water (3%–45%, both eluents were added with 0.1% FA); the system was washed with 90% of acetonitrile for 10 min and then re-equilibrated at 3% of acetonitrile for 18 min. The eluted peptides were analyzed by a TripleTof 5600+ mass spectrometer equipped with a NanoSpray III ion source and operating in data-independent acquisition (DIA) mode, following the SWATH protocol for label-free proteomics.[55] The instrument operated in positive ion mode with the following settings: ion spray voltage at 2,000 V, spray gas 1 at 14, curtain gas at 30, declustering potential at 80 V, and source temperature at 90°C. For protein quantification, the tandem mass (MS/MS) spectra were searched against a modified version of the PanHuman ion library, using only no-shared peptides.[55] The following parameters were used: minimum peptide confidence 90%, 50 ppm maximum mass tolerance, 30 min maximum RT tolerance, 6 MRM transitions per peptide, and modified peptides were not allowed.

In vivo *sample preparation*

Tumoral tissue from GBM xenotransplanted mice was harvested 2 weeks after treatment (ApoE-LNP injection), as described for *in vivo* transcriptomics samples (aforementioned); samples from $n = 3$ POOL-treated and $n = 3$ scrambled-treated animals were analyzed in technical triplicate. Tissue was lysed in RIPA buffer, homogenized by immersion sonication, and processed for protein digestion. 50 μg of proteins (quantified using the colorimetric Bradford dye-binding method, Bio-Rad kit) per sample was processed as follows: Cysteine residues were reduced/alkylated with a final concentration of 10 mM TCEP and 30 mM chloroacetamide (95°C for 15 min in the dark). After cooling at room temperature, samples were digested following the SP3 procedure, the concentration of the resulting peptides was measured (Fluorometric Peptide Assay, Thermo Fisher Scientific), and 300 ng of peptides was used for each analysis.[56]

LC-MS proteomics

Analysis was conducted on a Thermo Exploris 480 Orbitrap system coupled with a Dionex Ultimate 3000 nano-LC system. After trapping and desalting, the tryptic peptides were loaded on an Aurora C18 column (75 mm × 250 mm, 1.6 μm particle size, Ion Opticks, Fitzroy, Australia) and separated using a linear gradient of acetonitrile in water (both added with 0.1% formic acid), from 3% to 41% in 1 h, followed by column cleaning and reconditioning. The flow rate was set to 300 nL/min. Total run time was 1.5 h. Injection volume was set to 1 μL. Peptides were analyzed in positive ESI mode, using a capillary voltage set to 2.0 kV. The RF lens was set to 40%, and the AGC target was set at 300%. Data acquisition was performed in data-independent mode (DIA) with a survey scan set from 400 to 1,000 m/z at 120,000 mass resolution, followed by MS/MS acquisition of 60 m/z transmission windows, each having a fixed 10 Da width. MS/MS spectra were acquired in HCD mode. All the collected MS/MS spectra were analyzed using Spectronaut (version 18), by running 2 separate DirectDIA analyses against the reference Homo Sapiens FASTA and Mus musculus database. Cysteine carbamidomethylation was selected as fixed modification; acetylation of protein N-Term and methionine oxidation were selected as variable modifications. Positive protein identifications were retained at 1% FDR threshold, and at least two proteotypic peptides were used for protein quantification.

Data analysis

Proteomics in vitro

Quantifications of LC-MS raw data were normalized using the most likely ratio method before the statistical analysis.[57] To detect significant changes at protein level, an unpaired, 2 tailed t test was performed, and a total of 351 proteins for GBM1 and 462 proteins for GBM2 were found to be significantly (p value < 0.05) altered.

Proteomics in vivo

Proteomic identification was assigned to 191,723 unique peptides, corresponding to 10,765 proteins. Of the total number of peptides, 113,168 were found to be proteotypically human, which enabled the identification of 6,231 human proteotypic proteins. Concomitantly, 68,245 peptides were found to be proteotypically mouse, amounting to 5,267 murine proteotypic protein sequences. Thence, statistical analyses, by the one-way ANOVA method, with a p value threshold of 0.05, were performed by a custom script written in MATLAB (MathWorks) on the human proteotypic sequences only, in order to mitigate murine host tissue contamination of the engrafted tumor tissue.

Small RNA-seq

Illumina raw data and the small-RNA FastQ files were processed for adapter content using Cutadapt (version 4.9); untrimmed reads whose coverage did not capture adapter content were merged with the Cutadapt output. The composite files were processed for tetramers, according to library manufacturer's instructions, and quantified with miRge3.0, which incorporates the miRNA Transcriptomic Open Project (miRTOP) mirGFF3 standardization of isomiR-miRNA reporting. Outputs were normalized to obtain TPM expression relative to each sample, for each detected miRNA species. TPM values for the 11 miRNAs were selected and plotted into a heatmap.

Poly(A) mRNA sequencing

Raw data were processed with CLC Genomic Workbench (QIAGEN) to perform differential expression analysis (POOL vs. scramble), and DEGs with p value < 0.05 were selected. For *in vivo transcriptomics* data, given the presence of mouse tissue contamination in the tumor samples, a human+mouse hybrid reference genome was created (both species' genomes concatenated) and

used for alignment; then, reads mapping on more than one species were filtered out, and the remaining 42,155 human genes were used for DEG analysis.

GO enrichment

Significantly downregulated protein lists were analyzed separately on DAVID Database v6.8 (https://davidbioinformatics.nih.gov); the whole human genome was used as background. DAVID algorithm uses EASE score probability (a modified Fisher's exact *p* value) for calculating a *p* value for gene enrichment; The GO terms were listed from the most significant using Benjamini-corrected *p* values.

PPI analysis and *k*-means clustering were performed with the STRING software (https://string-db.org).[58]

TCGA database

GlioVis Data Visualization Tool for Brain Tumor Datasets (http://gliovis.bioinfo.cnio.es) was employed to analyze and download mRNA expression data encoding the 8 downregulated genes. TCGA RNA-seq dataset TCGA_GBMLGG was used for the correlation analysis of the genes of interest with glioma grade and patient survival.

Cell type cluster analysis

Cluster markers and cell type interpretation data from Bhaduri et al. were employed to obtain the lists of marker genes for each cluster.[2] For proteomics, non-significant marker genes were filtered out selecting only adjusted *p* values lower than 0.05; then, protein-coding gene lists obtained by proteomics data for both PD-GBM (i.e.,: total proteome list in ctrl-treated samples; significantly downregulated protein list; significantly upregulated protein list) were compared with each cluster's marker gene list to obtain the number of genes in common. Non-relevant cell type clusters (B cells, dividing B cells, and red blood cells) were removed from the analysis. The analysis was performed with R statistics. For *in vitro* transcriptomics, normalized counts were obtained with DESeq2, and cell clusters markers were used to create custom gene sets to be employed for GSEA with GSEA software.

miRNA-target prediction analysis was performed with DIANA tools (DIANA-microT 2023 webserver)[25]; validated miRNA-target interactions were retrieved from miRTarBase.[59]

DATA AND CODE AVAILABILITY

RNA datasets are available in the GEO database (GSE290046: https://www.ncbi.nlm.nih.gov/geo/query/acc.cgi?acc=GSE290046 and GSE290047: https://www.ncbi.nlm.nih.gov/geo/query/acc.cgi?acc=GSE290047). Proteomics data are available at PRIDE database (accession # PXD020335).

ACKNOWLEDGMENTS

The authors wish to thank M. Ghibaudi and F. Macchi for setting up the initial xenotransplantation experiments and M. Morini, E. Petrini, D. Vozzi, and the technical staff at IIT's Animal, Neurofacility, and Genomics facility for excellent support. We also wish to thank P. Malatesta at the IRCCS San Martino Hospital in Genoa and all the colleagues at the Neurobiology of miRNA lab of IIT for advice and discussion. This work was funded by IIT and partly by the grant AIRC-IG 2017 # 20106, by the project "National Center for Gene Therapy and Drug based on RNA Technology" (CN00000041) to D.D.P.T., and by the project MNESYS (PE0000006) – A multiscale integrated approach to the study of the nervous system in health and disease (DN. 1553 11.10.2022) to T.F. funded by the Ministry of University and Research (MUR), National Recovery and Resilience Plan (NRRP) #NEXTGENERATIONEU (NGEU). We apologize to those colleagues whose work could not be cited due to space limitations.

AUTHOR CONTRIBUTIONS

S.R., P.D., and D.D.P.T. designed research and experiments. S.R., S.S., R.C.P., M.S., S.B., L.L.R., L.G., R.P., C.B., A.D.F., C.S., A.L.V., M.P.-E., and A.P. performed the experiments. S.R., S.S., R.C.P., M.S., C.B., A.D.F., C.S., K.T., and A.L.V. performed data acquisition and analyses. S.R., S.S., and D.D.P.T. drafted the manuscript. K.T., A.A., P.D., T.F., and D.D.P.T. supervised the study. A.D., A.B., and T.F. provided glioblastoma cultures along with pathological and clinical data from patients. D.D.P.T. acquired funding. All authors read, revised, and approved the final version of the manuscript.

DECLARATION OF INTERESTS

The POOL of 11 miRNA is subject of the Italian priority patent application no. IT102016000093825, filed by D.D.P.T. and M.P.-E. on September 19, 2016, titled "A miRNAs pharmaceutical composition and its therapeutic uses" and subsequently filed as the international patents EP 17784688.8, US 16/331546, CA 3037254, and JP 2019-515210.

SUPPLEMENTAL INFORMATION

Supplemental information can be found online at https://doi.org/10.1016/j.omtn.2025.102763.

REFERENCES

1. Stupp, R., Mason, W.P., van den Bent, M.J., Weller, M., Fisher, B., Taphoorn, M.J.B., Belanger, K., Brandes, A.A., Marosi, C., Bogdahn, U., et al. (2005). Radiotherapy plus concomitant and adjuvant temozolomide for glioblastoma. N. Engl. J. Med. *352*, 987–996. https://doi.org/10.1056/NEJMoa043330.

2. Bhaduri, A., Di Lullo, E., Jung, D., Müller, S., Crouch, E.E., Espinosa, C.S., Ozawa, T., Alvarado, B., Spatazza, J., Cadwell, C.R., et al. (2020). Outer Radial Glia-like Cancer Stem Cells Contribute to Heterogeneity of Glioblastoma. Cell Stem Cell *26*, 48–63.e6. https://doi.org/10.1016/j.stem.2019.11.015.

3. Wang, R., Sharma, R., Shen, X., Laughney, A.M., Funato, K., Clark, P.J., Shpokayte, M., Morgenstern, P., Navare, M., Xu, Y., et al. (2020). Adult Human Glioblastomas Harbor Radial Glia-like Cells. Stem Cell Rep. *14*, 338–350. https://doi.org/10.1016/j.stemcr.2020.01.007.

4. Galli, R., Binda, E., Orfanelli, U., Cipelletti, B., Gritti, A., De Vitis, S., Fiocco, R., Foroni, C., Dimeco, F., and Vescovi, A. (2004). Isolation and Characterization of Tumorigenic, Stem-like Neural Precursors from Human Glioblastoma. Cancer Res. *64*, 7011–7021. https://doi.org/10.1158/0008-5472.CAN-04-1364.

5. Ignatova, T.N., Kukekov, V.G., Laywell, E.D., Suslov, O.N., Vrionis, F.D., and Steindler, D.A. (2002). Human cortical glial tumors contain neural stem-like cells expressing astroglial and neuronal markers in vitro. Glia *39*, 193–206. https://doi.org/10.1002/glia.10094.

6. Verhaak, R.G.W., Hoadley, K.A., Purdom, E., Wang, V., Qi, Y., Wilkerson, M.D., Miller, C.R., Ding, L., Golub, T., Mesirov, J.P., et al. (2010). Integrated genomic analysis identifies clinically relevant subtypes of glioblastoma characterized by abnormalities in PDGFRA, IDH1, EGFR, and NF1. Cancer Cell *17*, 98–110. https://doi.org/10.1016/j.ccr.2009.12.020.

7. Wang, Q., Hu, B., Hu, X., Kim, H., Squatrito, M., Scarpace, L., deCarvalho, A.C., Lyu, S., Li, P., Li, Y., et al. (2018). Tumor Evolution of Glioma-Intrinsic Gene Expression Subtypes Associates with Immunological Changes in the Microenvironment. Cancer Cell *33*, 152–156.e46. https://doi.org/10.1016/j.ccell.2017.12.012.

8. Hanahan, D., and Weinberg, R.A. (2011). Hallmarks of cancer: the next generation. Cell *144*, 646–674. https://doi.org/10.1016/j.cell.2011.02.013.

9. Friedman, R.C., Farh, K.K.H., Burge, C.B., and Bartel, D.P. (2009). Most mammalian mRNAs are conserved targets of microRNAs. Genome Res. *19*, 92–105. https://doi.org/10.1101/gr.082701.108.

10. Schmiedel, J.M., Klemm, S.L., Zheng, Y., Sahay, A., Blüthgen, N., Marks, D.S., and van Oudenaarden, A. (2015). Gene expression. MicroRNA control of protein expression noise. Science *348*, 128–132. https://doi.org/10.1126/science.aaa1738.

11. Siciliano, V., Garzilli, I., Fracassi, C., Criscuolo, S., Ventre, S., and di Bernardo, D. (2013). MiRNAs confer phenotypic robustness to gene networks by suppressing biological noise. Nat. Commun. *4*, 2364. https://doi.org/10.1038/ncomms3364.

12. Calin, G.A., Dumitru, C.D., Shimizu, M., Bichi, R., Zupo, S., Noch, E., Aldler, H., Rattan, S., Keating, M., Rai, K., et al. (2002). Frequent deletions and down-regulation of micro- RNA genes miR15 and miR16 at 13q14 in chronic lymphocytic leukemia. Proc. Natl. Acad. Sci. USA *99*, 15524–15529. https://doi.org/10.1073/pnas.242606799.

13. Silber, J., Lim, D.A., Petritsch, C., Persson, A.I., Maunakea, A.K., Yu, M., Vandenberg, S.R., Ginzinger, D.G., James, C.D., Costello, J.F., et al. (2008). miR-124 and miR-137 inhibit proliferation of glioblastoma multiforme cells and induce differentiation of brain tumor stem cells. BMC Med. *6*, 14. https://doi.org/10.1186/1741-7015-6-14.

14. Shahar, T., Granit, A., Zrihan, D., Canello, T., Charbit, H., Einstein, O., Rozovski, U., Elgavish, S., Ram, Z., Siegal, T., and Lavon, I. (2016). Expression level of miRNAs on chromosome 14q32.31 region correlates with tumor aggressiveness and survival of glioblastoma patients. J. Neuro Oncol. *130*, 413–422. https://doi.org/10.1007/s11060-016-2248-0.

15. Calvin, N., and Aman, R.A. (2024). Optimizing glioblastoma treatment: A systematic review and meta-analysis of local injection and systemic drug delivery system in murine models. Surg. Neurol. Int. *15*, 428. https://doi.org/10.25259/sni_588_2024.

16. Rupaimoole, R., and Slack, F.J. (2017). MicroRNA therapeutics: towards a new era for the management of cancer and other diseases. Nat. Rev. Drug Discov. *16*, 203–222. https://doi.org/10.1038/nrd.2016.246.

17. Kim, T., and Croce, C.M. (2023). MicroRNA: trends in clinical trials of cancer diagnosis and therapy strategies. Exp. Mol. Med. *55*, 1314–1321. https://doi.org/10.1038/s12276-023-01050-9.

18. Kosti, A., Barreiro, R., Guardia, G.D.A., Ostadrahimi, S., Kokovay, E., Pertsemlidis, A., Galante, P.A.F., and Penalva, L.O.F. (2021). Synergism of Proneurogenic miRNAs Provides a More Effective Strategy to Target Glioma Stem Cells. Cancers (Basel) *13*, 289. https://doi.org/10.3390/cancers13020289.

19. Bhaskaran, V., Nowicki, M.O., Idriss, M., Jimenez, M.A., Lugli, G., Hayes, J.L., Mahmoud, A.B., Zane, R.E., Passaro, C., Ligon, K.L., et al. (2019). The functional synergism of microRNA clustering provides therapeutically relevant epigenetic interference in glioblastoma. Nat. Commun. *10*, 442. https://doi.org/10.1038/s41467-019-08390-z.

20. McDonald, M.F., Hossain, A., Momin, E.N., Hasan, I., Singh, S., Adachi, S., Gumin, J., Ledbetter, D., Yang, J., Long, L., et al. (2024). Tumor-specific polycistronic miRNA delivered by engineered exosomes for the treatment of glioblastoma. Neuro Oncol. *26*, 236–250. https://doi.org/10.1093/neuonc/noad199.

21. Wang, C., Fu, R., Wang, Y., Wei, J., Yu, Y., Hu, L., and Zhang, C. (2024). miR-124-3p and miR-194-5p regulation of the PI3K/AKT pathway via ROR2 in medulloblastoma progression. Cancer Gene Ther. *31*, 941–954. https://doi.org/10.1038/s41417-024-00762-y.

22. Das, N., Bhat, S., Fugo, P., and Dhawan, A. (2025). miRNAs as neuro-oncologic therapeutics: A narrative review. Mol. Ther. *33*, 2740–2752. https://doi.org/10.1016/j.ymthe.2024.12.045.

23. Penning, A., Tosoni, G., Abiega, O., Bielefeld, P., Gasperini, C., De Pietri Tonelli, D., Fitzsimons, C.P., and Salta, E. (2021). Adult Neural Stem Cell Regulation by Small Non-coding RNAs: Physiological Significance and Pathological Implications. Front. Cell. Neurosci. *15*, 781434. https://doi.org/10.3389/fncel.2021.781434.

24. Pons-Espinal, M., de Luca, E., Marzi, M.J., Beckervordersandforth, R., Armirotti, A., Nicassio, F., Fabel, K., Kempermann, G., and De Pietri Tonelli, D. (2017). Synergic Functions of miRNAs Determine Neuronal Fate of Adult Neural Stem Cells. Stem Cell Rep. *8*, 1046–1061. https://doi.org/10.1016/j.stemcr.2017.02.012.

25. Kavakiotis, I., Alexiou, A., Tastsoglou, S., Vlachos, I.S., and Hatzigeorgiou, A.G. (2022). DIANA-miTED: a microRNA tissue expression database. Nucleic Acids Res. *50*, D1055–D1061. https://doi.org/10.1093/nar/gkab733.

26. Lim, Y., Beane-Ebel, J.E., Tanaka, Y., Ning, B., Husted, C.R., Henderson, D.C., Xiang, Y., Park, I.-H., Farrer, L.A., and Zhang, H. (2021). Exploration of alcohol use disorder-associated brain miRNA–mRNA regulatory networks. Transl. Psychiatry *11*, 504. https://doi.org/10.1038/s41398-021-01635-w.

27. Griffero, F., Daga, A., Marubbi, D., Capra, M.C., Melotti, A., Pattarozzi, A., Gatti, M., Bajetto, A., Porcile, C., Barbieri, F., et al. (2009). Different Response of Human Glioma Tumor-initiating Cells to Epidermal Growth Factor Receptor Kinase Inhibitors. J. Biol. Chem. *284*, 7138–7148. https://doi.org/10.1074/jbc.M807111200.

28. Pereira, R.C., Santagiuliana, R., Ceseracciu, L., Boso, D.P., Schrefler, B.A., and Decuzzi, P. (2020). Elucidating the Role of Matrix Porosity and Rigidity in Glioblastoma Type IV Progression. Applied Sciences *10*, 9076. https://doi.org/10.3390/app10249076.

29. Lee, J., Kotliarova, S., Kotliarov, Y., Li, A., Su, Q., Donin, N.M., Pastorino, S., Purow, B.W., Christopher, N., Zhang, W., et al. (2006). Tumor stem cells derived from glioblastomas cultured in bFGF and EGF more closely mirror the phenotype and genotype of primary tumors than do serum-cultured cell lines. Cancer Cell *9*, 391–403. https://doi.org/10.1016/j.ccr.2006.03.030.

30. Lazzarini, E., Silvestris, D.A., Benvenuto, G., Osti, D., Fattore, L., Paterra, R., Finocchiaro, G., Malatesta, P., Daga, A., Gallotti, A.L., et al. (2023). Genome-wide profiling of patient-derived glioblastoma stem-like cells reveals recurrent genetic and transcriptomic signatures associated with brain tumors. J. Neuro Oncol. *163*, 47–59. https://doi.org/10.1007/s11060-023-04287-6.

31. Kim, Y., Varn, F.S., Park, S.-H., Yoon, B.W., Park, H.R., Lee, C., Verhaak, R.G.W., and Paek, S.H. (2021). Perspective of mesenchymal transformation in glioblastoma. Acta Neuropathol. Commun. *9*, 50. https://doi.org/10.1186/s40478-021-01151-4.

32. Vasilogiannakopoulou, T., Piperi, C., and Papavassiliou, A.G. (2018). Impact of Aldehyde Dehydrogenase Activity on Gliomas. Trends Pharmacol. Sci. *39*, 605–609. https://doi.org/10.1016/j.tips.2018.04.001.

33. Nowakowski, T.J., Bhaduri, A., Pollen, A.A., Alvarado, B., Mostajo-Radji, M.A., Di Lullo, E., Haeussler, M., Sandoval-Espinosa, C., Liu, S.J., Velmeshev, D., et al. (2017). Spatiotemporal gene expression trajectories reveal developmental hierarchies of the human cortex. Science *358*, 1318–1323. https://doi.org/10.1126/science.aap8809.

34. Ricci-Vitiani, L., Pallini, R., Biffoni, M., Todaro, M., Invernici, G., Cenci, T., Maira, G., Parati, E.A., Stassi, G., Larocca, L.M., and De Maria, R. (2010). Tumour vascularization via endothelial differentiation of glioblastoma stem-like cells. Nature *468*, 824–828. https://doi.org/10.1038/nature09557.

35. Coelho, T., Adams, D., Silva, A., Lozeron, P., Hawkins, P.N., Mant, T., Perez, J., Chiesa, J., Warrington, S., Tranter, E., et al. (2013). Safety and efficacy of RNAi therapy for transthyretin amyloidosis. N. Engl. J. Med. *369*, 819–829. https://doi.org/10.1056/NEJMoa1208760.

36. Cohen, Z.R., Ramishetti, S., Peshes-Yaloz, N., Goldsmith, M., Wohl, A., Zibly, Z., and Peer, D. (2015). Localized RNAi therapeutics of chemoresistant grade IV glioma using hyaluronan-grafted lipid-based nanoparticles. ACS Nano *9*, 1581–1591. https://doi.org/10.1021/nn506248s.

37. Maletínská, L., Blakely, E.A., Bjornstad, K.A., Deen, D.F., Knoff, L.J., and Forte, T.M. (2000). Human glioblastoma cell lines: levels of low-density lipoprotein receptor and low-density lipoprotein receptor-related protein. Cancer Res. *60*, 2300–2303.

38. Rungta, R.L., Choi, H.B., Lin, P.J., Ko, R.W., Ashby, D., Nair, J., Manoharan, M., Cullis, P.R., and Macvicar, B.A. (2013). Lipid Nanoparticle Delivery of siRNA to Silence Neuronal Gene Expression in the Brain. Mol. Ther. Nucleic Acids *2*, e136. https://doi.org/10.1038/mtna.2013.65.

39. Harwood, D.S.L., Pedersen, V., Bager, N.S., Schmidt, A.Y., Stannius, T.O., Areškevičiūtė, A., Josefsen, K., Nørøxe, D.S., Scheie, D., Rostalski, H., et al. (2024). Glioblastoma cells increase expression of notch signaling and synaptic genes within infiltrated brain tissue. Nat. Commun. *15*, 7857. https://doi.org/10.1038/s41467-024-52167-y.

40. Venkataramani, V., Yang, Y., Schubert, M.C., Reyhan, E., Tetzlaff, S.K., Wißmann, N., Botz, M., Soyka, S.J., Beretta, C.A., Pramatarov, R.L., et al. (2022). Glioblastoma hijacks neuronal mechanisms for brain invasion. Cell *185*, 2899–2917.e31. https://doi.org/10.1016/j.cell.2022.06.054.

41. Li, R., Tao, T., Ren, Q., Xie, S., Gao, X., Wu, J., Chen, D., and Xu, C. (2022). Key Genes Are Associated with the Prognosis of Glioma, and Melittin Can Regulate the Expression of These Genes in Glioma U87 Cells. BioMed Res. Int. *2022*, 7033478. https://doi.org/10.1155/2022/7033478.

42. Gao, Y.F., Mao, X.Y., Zhu, T., Mao, C.X., Liu, Z.X., Wang, Z.B., Li, L., Li, X., Yin, J.Y., Zhang, W., et al. (2016). COL3A1 and SNAP91: novel glioblastoma markers with diagnostic and prognostic value. Oncotarget *7*, 70494–70503. https://doi.org/10.18632/oncotarget.12038.

43. Shi, Y., Wu, M., Liu, Y., Hu, L., Wu, H., Xie, L., Liu, Z., Wu, A., Chen, L., and Xu, C. (2021). ITGA5 Predicts Dual-Drug Resistance to Temozolomide and Bevacizumab in Glioma. Front. Oncol. *11*, 769592. https://doi.org/10.3389/fonc.2021.769592.

44. Kabir, F., and Apu, M.N.H. (2022). Multi-omics analysis predicts fibronectin 1 as a prognostic biomarker in glioblastoma multiforme. Genomics *114*, 110378. https://doi.org/10.1016/j.ygeno.2022.110378.

45. Chokshi, C.R., Shaikh, M.V., Brakel, B., Rossotti, M.A., Tieu, D., Maich, W., Anand, A., Chafe, S.C., Zhai, K., Suk, Y., et al. (2024). Targeting axonal guidance dependencies in glioblastoma with ROBO1 CAR T cells. Nat. Med. *30*, 2936–2946. https://doi.org/10.1038/s41591-024-03138-9.

46. Xue, B.Z., Xiang, W., Zhang, Q., Wang, H.F., Zhou, Y.J., Tian, H., Abdelmaksou, A., Xue, J., Sun, M.X., Yi, D.Y., et al. (2021). CD90(low) glioma-associated mesenchymal stromal/stem cells promote temozolomide resistance by activating FOXS1-mediated epithelial-mesenchymal transition in glioma cells. Stem Cell Res. Ther. *12*, 394. https://doi.org/10.1186/s13287-021-02458-8.

47. Tao, B., Song, Y., Wu, Y., Yang, X., Peng, T., Peng, L., Xia, K., Xia, X., Chen, L., and Zhong, C. (2021). Matrix stiffness promotes glioma cell stemness by activating BCL9L/Wnt/β-catenin signaling. Aging (Albany NY) *13*, 5284–5296. https://doi.org/10.18632/aging.202449.

48. Miller, T.E., Liau, B.B., Wallace, L.C., Morton, A.R., Xie, Q., Dixit, D., Factor, D.C., Kim, L.J.Y., Morrow, J.J., Wu, Q., et al. (2017). Transcription elongation factors represent in vivo cancer dependencies in glioblastoma. Nature *547*, 355–359. https://doi.org/10.1038/nature23000.

49. Sperring, C.P., Argenziano, M.G., Savage, W.M., Teasley, D.E., Upadhyayula, P.S., Winans, N.J., Canoll, P., and Bruce, J.N. (2023). Convection-enhanced delivery of immunomodulatory therapy for high-grade glioma. Neurooncol. Adv. *5*, vdad044. https://doi.org/10.1093/noajnl/vdad044.

50. Di Mascolo, D., Palange, A.L., Primavera, R., Macchi, F., Catelani, T., Piccardi, F., Spanò, R., Ferreira, M., Marotta, R., Armirotti, A., et al. (2021). Conformable hierarchically engineered polymeric micromeshes enabling combinatorial therapies in brain tumours. Nat. Nanotechnol. *16*, 820–829. https://doi.org/10.1038/s41565-021-00879-3.

51. Yuen, J.G., Fesler, A., Hwang, G.R., Chen, L.B., and Ju, J. (2022). Development of 5-FU-modified tumor suppressor microRNAs as a platform for novel microRNA-based cancer therapeutics. Mol. Ther. *30*, 3450–3461. https://doi.org/10.1016/j.ymthe.2022.07.015.

52. Kian, R., Moradi, S., and Ghorbian, S. (2018). Role of components of microRNA machinery in carcinogenesis. Exp. Oncol. *40*, 2–9.

53. Hambardzumyan, D., and Bergers, G. (2015). Glioblastoma: Defining Tumor Niches. Trends Cancer *1*, 252–265. https://doi.org/10.1016/j.trecan.2015.10.009.

54. Castellan, M., Guarnieri, A., Fujimura, A., Zanconato, F., Battilana, G., Panciera, T., Sladitschek, H.L., Contessotto, P., Citron, A., Grilli, A., et al. (2021). Single-cell analyses reveal YAP/TAZ as regulators of stemness and cell plasticity in Glioblastoma. Nat. Cancer *2*, 174–188. https://doi.org/10.1038/s43018-020-00150-z.

55. Braccia, C., Tomati, V., Caci, E., Pedemonte, N., and Armirotti, A. (2019). SWATH label-free proteomics for cystic fibrosis research. J. Cyst. Fibros. *18*, 501–506. https://doi.org/10.1016/j.jcf.2018.10.004.

56. Hughes, C.S., Moggridge, S., Müller, T., Sorensen, P.H., Morin, G.B., and Krijgsveld, J. (2019). Single-pot, solid-phase-enhanced sample preparation for proteomics experiments. Nat. Protoc. *14*, 68–85. https://doi.org/10.1038/s41596-018-0082-x.

57. Huang, Q., Yang, L., Luo, J., Guo, L., Wang, Z., Yang, X., Jin, W., Fang, Y., Ye, J., Shan, B., and Zhang, Y. (2015). SWATH enables precise label-free quantification on proteome scale. Proteomics *15*, 1215–1223. https://doi.org/10.1002/pmic.201400270.

58. Szklarczyk, D., Kirsch, R., Koutrouli, M., Nastou, K., Mehryary, F., Hachilif, R., Gable, A.L., Fang, T., Doncheva, N.T., Pyysalo, S., et al. (2023). The STRING database in 2023: protein-protein association networks and functional enrichment analyses for any sequenced genome of interest. Nucleic Acids Res. *51*, D638–D646. https://doi.org/10.1093/nar/gkac1000.

59. Huang, H.Y., Lin, Y.C.D., Cui, S., Huang, Y., Tang, Y., Xu, J., Bao, J., Li, Y., Wen, J., Zuo, H., et al. (2022). miRTarBase update 2022: an informative resource for experimentally validated miRNA-target interactions. Nucleic Acids Res. *50*, D222–D230. https://doi.org/10.1093/nar/gkab1079.